Computers and Structures 237 (2020) 106273

Contents lists available at ScienceDirect

Computers and Structures

journal homepage: www.elsevier.com/locate/compstruc

Transient wave propagation in inhomogeneous media with enriched overlapping triangular elements

Yingbin Chai, Klaus-Jürgen Bathe *

Department of Mechanical Engineering, Massachusetts Institute of Technology, Cambridge, MA 02139, USA

ARTICLE INFO

Article history:
Received 4 March 2020
Accepted 23 April 2020

Keywords:
Wave propagations
Inhomogeneous media
Finite elements
Overlapping finite elements
Numerical dispersion
Bathe time integration

ABSTRACT

We study and use overlapping triangular finite elements enriched by trigonometric functions and implicit time integration to solve transient wave propagations in inhomogeneous media. We show explicitly that the total dispersion error of the calculated solutions can be split into two parts, the spatial error and temporal error. The study of the spatial dispersion error shows the effectiveness of the enriched overlapping finite elements compared to the traditional finite elements and the overlapping finite elements without enrichment. The study of the temporal error of the Bathe time integration scheme shows monotonic convergence to zero with decreasing time step size. The result is that we see monotonic convergence to exact solutions as the mesh of enriched overlapping finite elements is refined and the time step is decreased. We demonstrate the effectiveness of using the proposed scheme in the solution of waves traveling in inhomogeneous media at different speeds, where reflected and transmitted waves are predicted accurately by "simply" using a fine enough mesh and small enough time step.

1. Introduction

The solution of transient wave propagation problems is of great importance in practical engineering analyses. Exact solutions can only be obtained for relatively simple problems, such as a single wave propagating in a one-dimensional space. Solutions of waves in complex geometric shapes can only be obtained by resorting to numerical methods.

The classical finite element method is a popular and widely used numerical approach for solving transient wave propagation problems. However, the solutions using the standard method suffer from significant dispersion errors induced by the spatial discretizations [1–5]. As a result, inaccurate numerical solutions are frequently obtained, especially in the relatively high wave number range. It is also found that the solutions show significant numerical anisotropy [5–7], that is, the accuracy of solutions depends on the directions of wave propagations even when the medium is isotropic and a seemingly uniform mesh is used.

Significant research efforts have focused on reducing the dispersion error in the solution of transient wave propagations in solids and various methods have been proposed, see e.g. [8–14], including the spectral element method, see e.g. [15–18]. This scheme is a higher-order numerical technique combining spectral methods and the classical finite element discretization. The spectral element method can be used to solve problems with much less numerical dispersion error than the traditional finite element method; however, the procedure is difficult to use to solve general two- and three-dimensional problems in complex geometries. This limitation significantly impedes its wider application in practical engineering computations.

The method of finite spheres [19,20], which is a typical meshfree numerical method, has also been proposed for wave propagation problems [12,13]. If uniform spatial discretizations are employed, the method of finite sphere is quite effective in eliminating the numerical dispersion error and numerical anisotropy. However, a main shortcoming of the method is that a very expensive numerical integration is required in constructing the system matrices for non-uniform spatial discretizations.

Recently, a new paradigm of using "overlapping elements" was proposed for general static and dynamic analyses of solids and structures [21–25]. Numerical results show that the procedure can provide much more accurate solutions than the traditional finite element method without an expensive computational effort. Quite importantly, it was shown that the predictive behavior of the overlapping finite elements is almost insensitive to the geometric distortions of the mesh. The reason is that the local interpolations used in the method are not affected by (reasonable) geometric distortions of the mesh. This property is very valuable, significantly distinguishes the overlapping finite element method from the tra-

* Corresponding author.
E-mail address: kjb@mit.edu (K.J. Bathe).

https://doi.org/10.1016/j.compstruc.2020.106273
0045-7949/

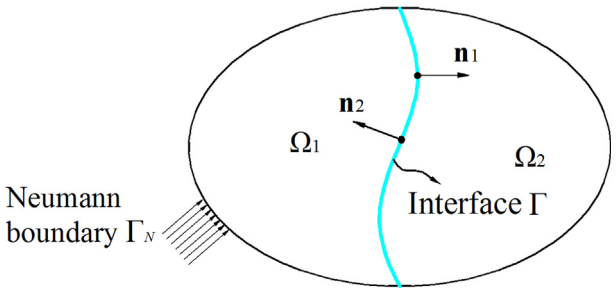

Fig. 1. General problem domain with different media.

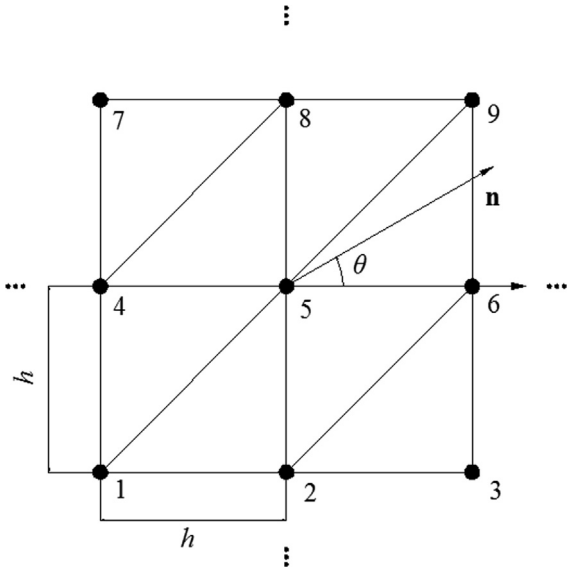

Fig. 2. The uniform mesh with triangular elements for dispersion analysis.

ditional finite element method, and makes the procedure an important ingredient in the AMORE scheme [24,25].

Kim et al. successfully used overlapping finite elements enriched by trigonometric functions to solve transient wave propagations in homogeneous media [14]. The numerical results demonstrated that the proposed enriched overlapping finite element method with the Bathe time integration scheme shows several excellent but related solution properties for wave propagation problems. The key property is that the solutions using the scheme monotonically converge to the exact solution as the element size and time step decrease. Namely, when using a sufficiently fine mesh and small time step, the numerical dispersion error and numerical anisotropy are small, which means also that when multiple waves travel through the medium, these can all be solved for accurately. The property of monotonic convergence is very useful in practical engineering computations because accurate solutions can be reached by "simply" using a sufficiently fine mesh (as in static analyses) and a sufficiently small time step.

We focus in this paper on exploring the application of the 'enriched overlapping finite elements' to solve transient wave propagation problems in inhomogeneous media. Our study adds to the results published earlier by Kim et al. [14] who considered homogeneous media. We give now new insights regarding the dispersion errors, and also show that using the enriched overlapping finite element discretization provides much more accurate solutions than when using traditional finite elements or the overlapping finite elements without enrichment. Based on our observations we can expect that the overlapping finite element method using enrichments has much potential in solving complex wave propagation problems involving also anisotropic and composite media.

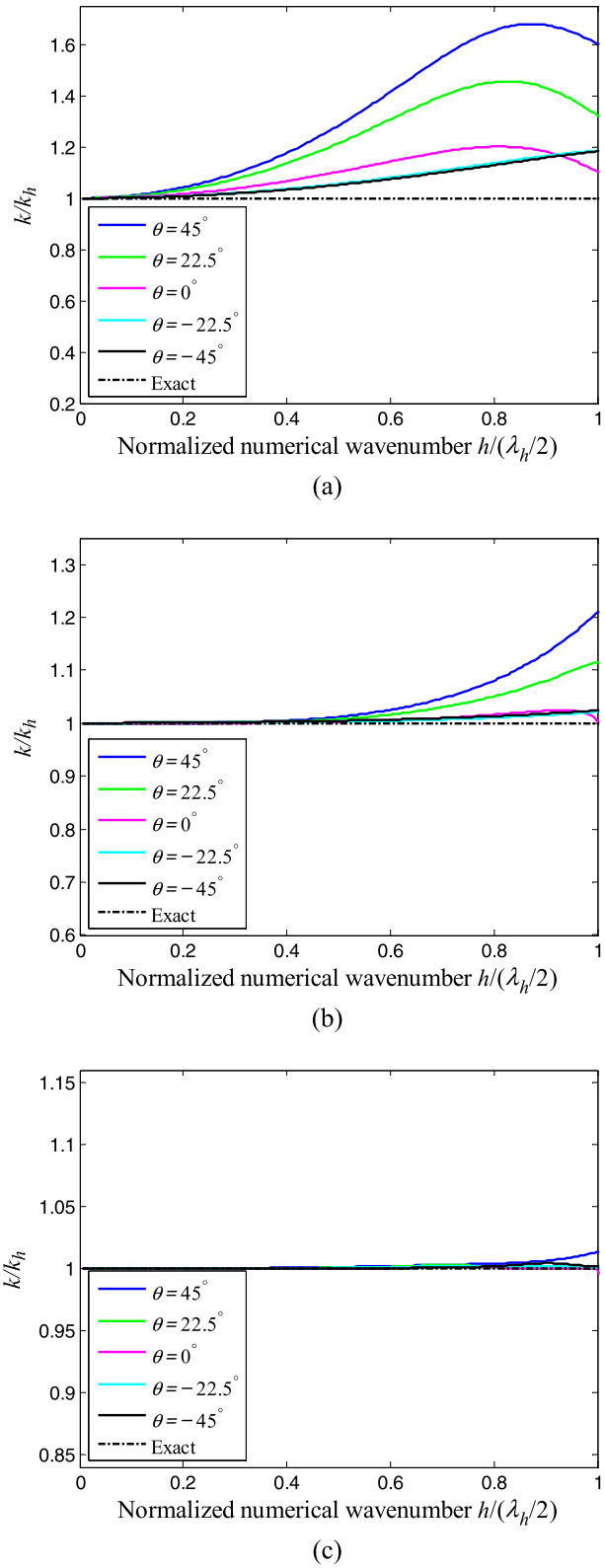

Fig. 3. Dispersion errors induced by spatial discretizations in various wave propagation directions: (a) FEM; (b) OFEM; (c) EOFEM.

2. Governing equations of wave propagation in inhomogeneous media.

We consider a general problem domain $\Omega = \Omega_1 \cup \Omega_2$ consisting of two sub-domains filled with two different media, as shown in Fig. 1. The governing wave equations are given as

$$\begin{cases} \nabla^2 u_1 - \frac{1}{c_1^2}\ddot{u}_1 = 0, & \text{in } \Omega_1 \\ \nabla^2 u_2 - \frac{1}{c_2^2}\ddot{u}_2 = 0, & \text{in } \Omega_2 \end{cases} \tag{1}$$

in which u_I ($I = 1, 2$) is the solution variable of wave propagation (such as pressure [26] or displacement [14]) in the sub-domains Ω_I, $I = 1, 2$; ∇^2 is the Laplace operator, c_I ($I = 1, 2$) is the wave propagation velocity in the different media, and an overdot represents a derivative with respect to time.

On the interface Γ of the two media, the solution needs to satisfy the following interface conditions

$$\begin{cases} u_1 = u_2 \\ v_1 = v_2 \end{cases}, \quad \text{on } \Gamma \tag{2}$$

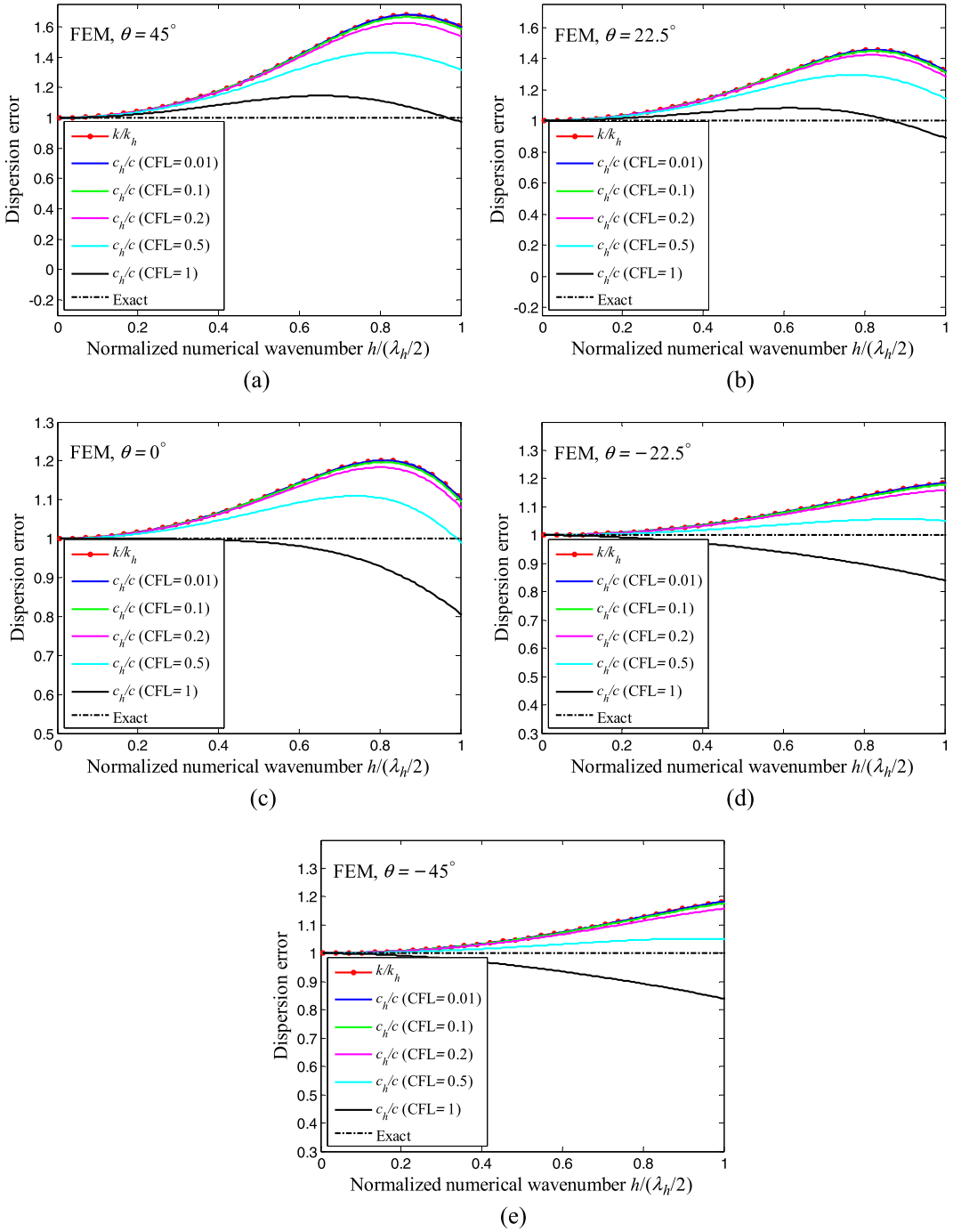

Fig. 4. Dispersion error of the standard FEM with Bathe time integration scheme for different CFL numbers: (a) $\theta = 45^\circ$; (b) $\theta = 22.5^\circ$; (c) $\theta = 0^\circ$; (d) $\theta = -22.5^\circ$; (e) $\theta = -45^\circ$.

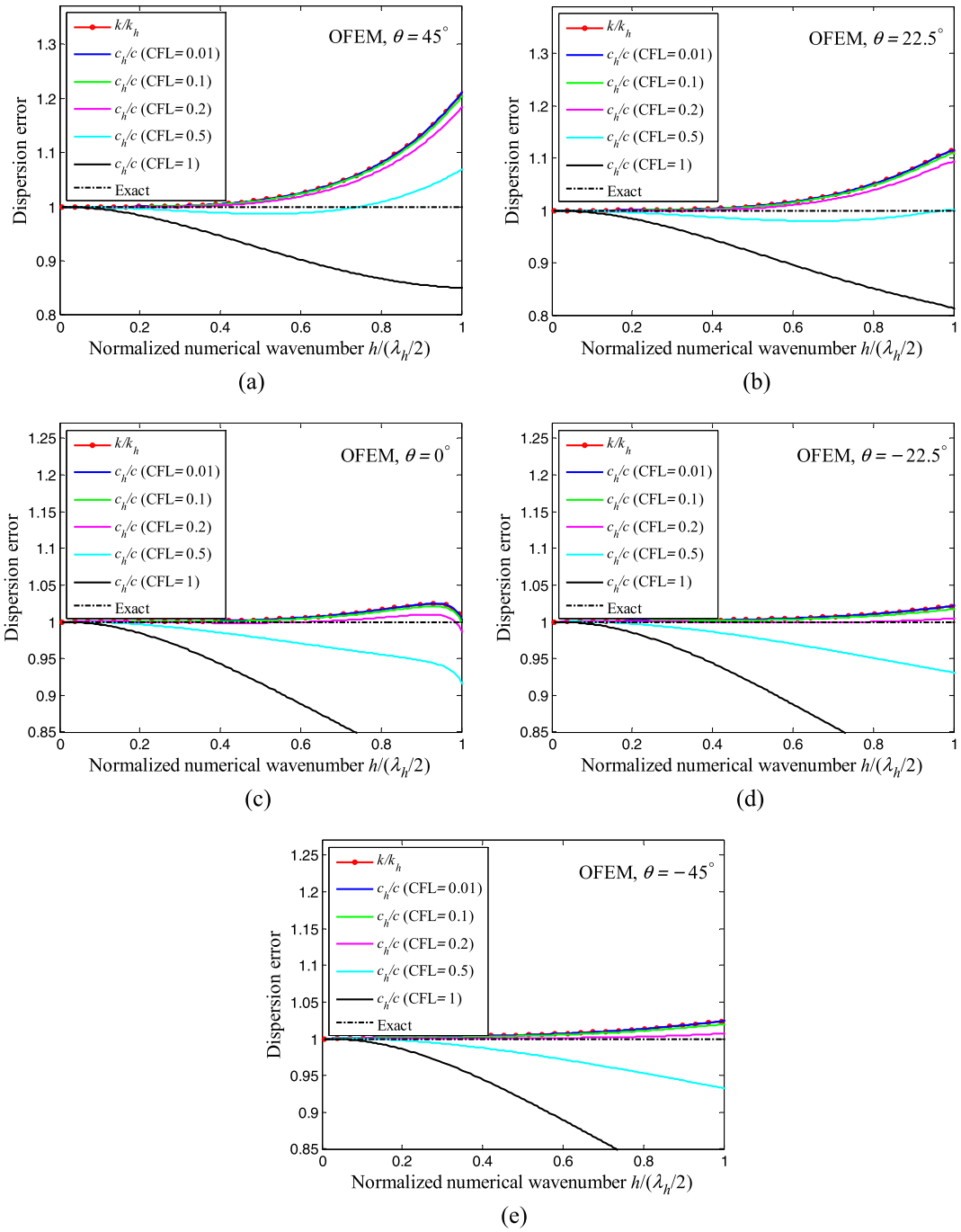

Fig. 5. Dispersion error of the standard OFEM with Bathe time integration scheme for different CFL numbers: (a) $\theta = 45^\circ$; (b) $\theta = 22.5^\circ$; (c) $\theta = 0^\circ$; (d) $\theta = -22.5^\circ$; (e) $\theta = -45^\circ$.

in which v_I ($I = 1, 2$) are the particle velocities on the interface Γ. These particle velocities are defined using normal directions to the interface.

For the wave propagation of pressure in an ideal acoustic fluid, the relationship between pressure u and particle velocity v is given by

$$\frac{\nabla u \cdot \mathbf{n}}{\rho} = \dot{v} \tag{3}$$

in which $\mathbf{n}$ is the outward normal unit vector to the interface and ρ is the density of the acoustic fluid.

For the wave propagation in a pre-stressed membrane, the relationship between displacement u and particle velocity v is given by

$$c\nabla u \cdot \mathbf{n} - v = 0 \tag{4}$$

in which c is the wave propagation velocity.

Using Eqs. (3) and (4), the interface conditions shown in Eq. (2) can be written as

$$\begin{cases} u_1 = u_2 \\ (\nabla u_1 \cdot \mathbf{n}_1) \cdot \alpha_1 + (\nabla u_2 \cdot \mathbf{n}_2) \cdot \alpha_2 = 0 \end{cases}, \quad \text{on } \Gamma \tag{5}$$

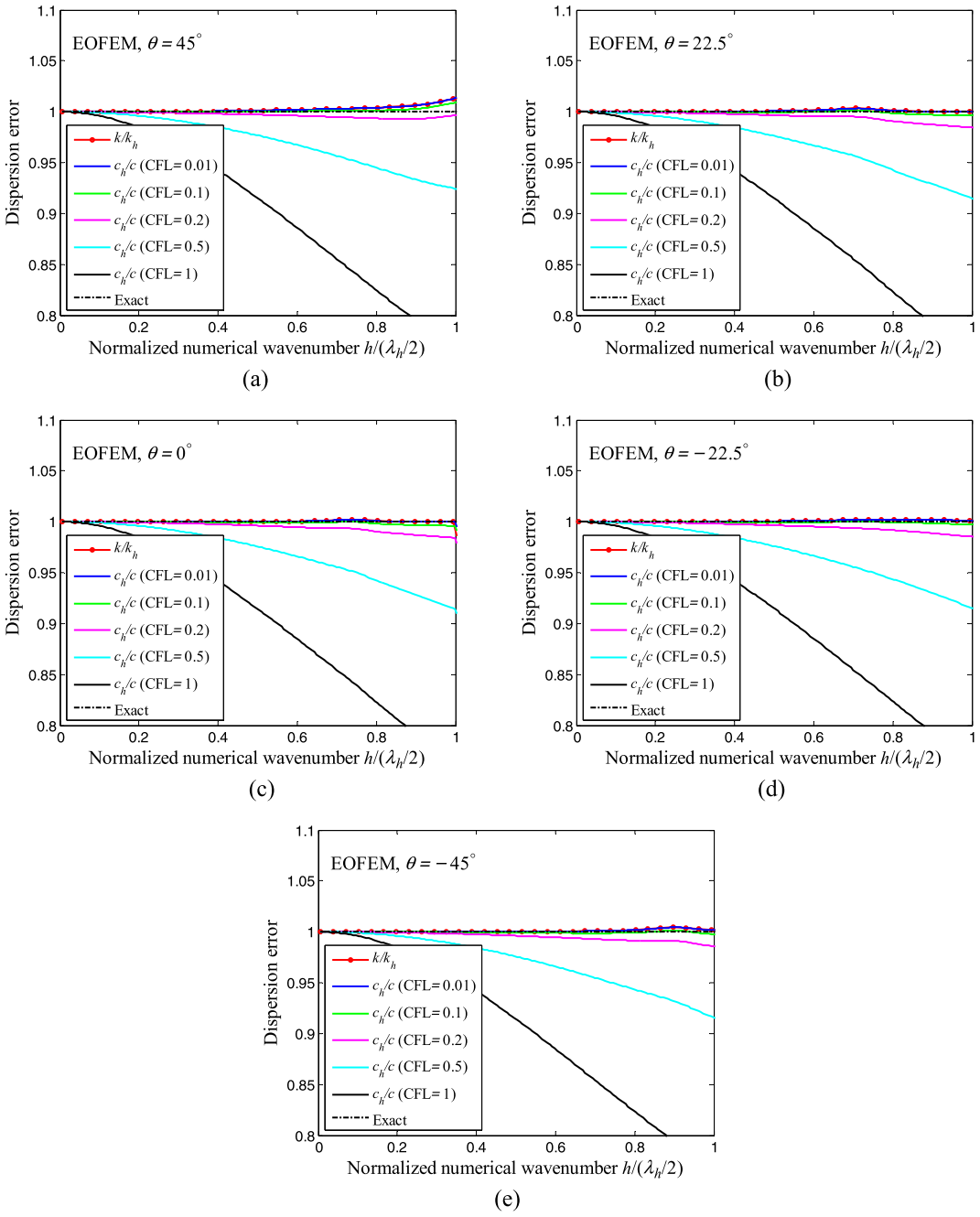

Fig. 6. Dispersion error of the EOFEM with Bathe time integration scheme for different CFL numbers: (a) $\theta = 45^\circ$; (b) $\theta = 22.5^\circ$; (c) $\theta = 0^\circ$; (d) $\theta = -22.5^\circ$; (e) $\theta = -45^\circ$.

in which $\alpha_I = \frac{1}{\rho_I}$ $(I = 1, 2)$ for the propagation of pressure in an ideal acoustic fluid, $\alpha_I = c_I$ $(I = 1, 2)$ for the wave propagation in pre-stressed membranes, and $\mathbf{n}_1, \mathbf{n}_2$ are the unit outward normal vectors to the interface for the sub-domains Ω_I, $I = 1, 2$, respectively (see Fig. 1). The directions of the normal vectors are important to be able to write Eq. (5).

Using the principle of virtual work for Eq. (1), we have [26]

$$\sum_{I=1}^{2} \int_{\Omega_I} \bar{u}\left(\nabla^2 u_I - \frac{1}{c_I^2}\ddot{u}_I\right) d\Omega = 0 \tag{6}$$

where $\bar{u}$ is the arbitrary "virtual pressure/displacement distribution".

Performing, as usual, integration by parts and using the divergence theorem, we obtain

$$\sum_{I=1}^{2}\left(\int_{\Omega_I} \nabla \bar{u} \cdot \nabla u_I d\Omega + \frac{1}{c_I^2}\int_{\Omega_I} \bar{u}\,\ddot{u}_I d\Omega - \int_{\Gamma_N} \bar{u}\,(\nabla u_I \cdot \mathbf{n}_I) d\Gamma\right) = 0 \tag{7}$$

in which we have on Γ_N the imposed Neumann boundary condition.

The principle of virtual work is equivalent to invoking the total potential energy Π corresponding to Eq. (7). We use Π and introduce the interface conditions of Eq. (2) by a Lagrange multiplier λ

$$\Pi^* = \Pi - \int_{\Gamma} \lambda((\nabla u_1 \cdot \mathbf{n}_1) \cdot \alpha_1 + (\nabla u_2 \cdot \mathbf{n}_2) \cdot \alpha_2) d\Gamma \tag{8}$$

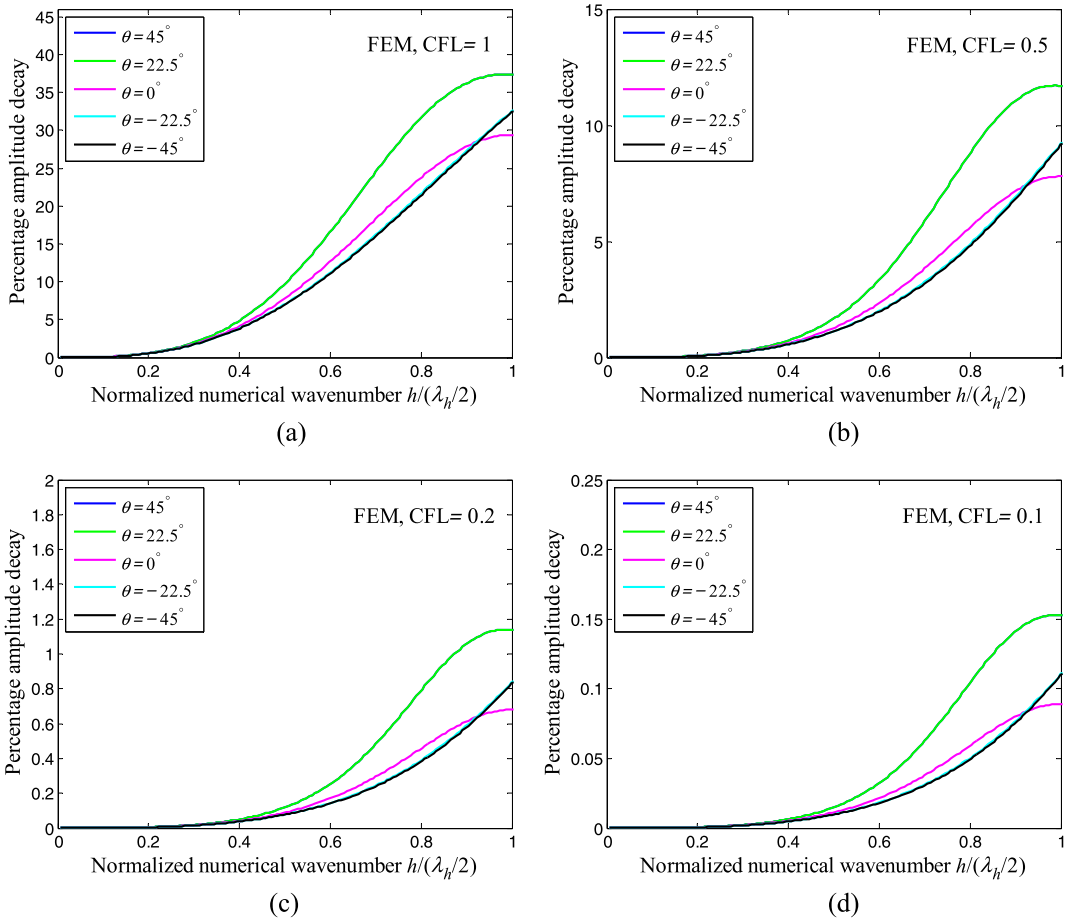

Fig. 7. Dissipation of the standard FEM with Bathe time integration scheme: (a) CFL = 1; (b) CFL = 0.5; (c) CFL = 0.2; (d) CFL = 0.1.

Invoking $\delta\Pi^* = 0$ and using the finite element interpolations, the corresponding matrices are obtained

$$\begin{cases} \frac{1}{c_1^2}\int_{\Omega_1}\mathbf{H}_{f_1}^T\mathbf{H}_{f_1}\ddot{\mathbf{U}}_1 d\Omega + \int_{\Omega_1}(\nabla\mathbf{H}_{f_1})^T\nabla\mathbf{H}_{f_1}\mathbf{U}_1 d\Omega \\ -\int_{\Gamma_N}\mathbf{H}_{f_1}^T(\nabla u_1\cdot\mathbf{n}_1)d\Gamma - \int_{\Gamma}(\nabla\mathbf{H}_{f_1})^T\cdot\mathbf{n}_1\mathbf{H}_\lambda\alpha_1\lambda d\Gamma = \mathbf{0} \\ \frac{1}{c_2^2}\int_{\Omega_2}\mathbf{H}_{f_2}^T\mathbf{H}_{f_2}\ddot{\mathbf{U}}_2 d\Omega + \int_{\Omega_2}(\nabla\mathbf{H}_{f_2})^T\nabla\mathbf{H}_{f_2}\mathbf{U}_2 d\Omega \\ -\int_{\Gamma_N}\mathbf{H}_{f_2}^T(\nabla u_2\cdot\mathbf{n}_2)d\Gamma - \int_{\Gamma}(\nabla\mathbf{H}_{f_2})^T\cdot\mathbf{n}_2\mathbf{H}_\lambda\alpha_2\lambda d\Gamma = \mathbf{0} \\ -\int_{\Gamma}\mathbf{H}_\lambda^T\mathbf{n}_1\cdot(\nabla\mathbf{H}_{f_1})\alpha_1\mathbf{U}_1 d\Gamma - \int_{\Gamma}\mathbf{H}_\lambda^T\mathbf{n}_2\cdot(\nabla\mathbf{H}_{f_2})\alpha_2\mathbf{U}_2 d\Gamma = \mathbf{0} \end{cases} \tag{9}$$

in which $\mathbf{H}_{f_1}$, $\mathbf{H}_{f_2}$ and $\mathbf{H}_\lambda$ contain the interpolation functions corresponding to the two sub-domains Ω_1 and Ω_2 and the interfaces Γ and Γ_N (see Fig. 1) and $\mathbf{U}_1$, $\mathbf{U}_2$, $\boldsymbol{\lambda}$ are the unknown nodal values to be calculated.

The above equations can be written as

$$\begin{bmatrix}\mathbf{M}_1 & \mathbf{0} & \mathbf{0}\\ \mathbf{0} & \mathbf{M}_2 & \mathbf{0}\\ \mathbf{0} & \mathbf{0} & \mathbf{0}\end{bmatrix}\begin{bmatrix}\ddot{\mathbf{U}}_1\\ \ddot{\mathbf{U}}_2\\ \ddot{\boldsymbol{\lambda}}\end{bmatrix} + \begin{bmatrix}\mathbf{K}_1 & \mathbf{0} & \mathbf{A}\\ \mathbf{0} & \mathbf{K}_2 & \mathbf{G}\\ \mathbf{A}^T & \mathbf{G}^T & \mathbf{0}\end{bmatrix}\begin{bmatrix}\mathbf{U}_1\\ \mathbf{U}_2\\ \boldsymbol{\lambda}\end{bmatrix} = \begin{bmatrix}\mathbf{R}_1\\ \mathbf{R}_2\\ \mathbf{0}\end{bmatrix} \tag{10}$$

in which

$$\begin{aligned} &\mathbf{M}_1 = \tfrac{1}{c_1^2}\int_{\Omega_1}\mathbf{H}_{f_1}^T\mathbf{H}_{f_1}d\Omega, && \mathbf{M}_2 = \tfrac{1}{c_2^2}\int_{\Omega_2}\mathbf{H}_{f_2}^T\mathbf{H}_{f_2}d\Omega\\ &\mathbf{K}_1 = \int_{\Omega_1}(\nabla\mathbf{H}_{f_1})^T\nabla\mathbf{H}_{f_1}d\Omega, && \mathbf{K}_2 = \int_{\Omega_2}(\nabla\mathbf{H}_{f_2})^T\nabla\mathbf{H}_{f_2}d\Omega\\ &\mathbf{A} = -\int_{\Gamma}(\nabla\mathbf{H}_{f_1})^T\cdot\mathbf{n}_1\mathbf{H}_\lambda\alpha_1 d\Gamma, && \mathbf{G} = -\int_{\Gamma}(\nabla\mathbf{H}_{f_2})^T\cdot\mathbf{n}_2\mathbf{H}_\lambda\alpha_2 d\Gamma\\ &\mathbf{R}_1 = \int_{\Gamma_N}\mathbf{H}_{f_1}^T(\nabla u_1\cdot\mathbf{n}_1)d\Gamma, && \mathbf{R}_2 = \int_{\Gamma_N}\mathbf{H}_{f_2}^T(\nabla u_2\cdot\mathbf{n}_2)d\Gamma \end{aligned} \tag{11}$$

3. The interpolation scheme of enriched overlapping elements

We use the enriched triangular overlapping elements [21–24]. For every overlap region with three nodes *I*, *L*, *M* the interpolation of the solution variable u is given by

$$u_h(\mathbf{x}) = \rho_I\mathbf{u}_I + \rho_L\mathbf{u}_L + \rho_M\mathbf{u}_M \tag{12}$$

in which, with $J = I, L, M$, the ρ_J are the new interpolation functions and the $\mathbf{u}_J$ are the nodal unknowns which can be functions.

The three new interpolation functions are given by

$$\rho_J = \phi_J^I\, h_I + \phi_J^L\, h_L + \phi_J^M\, h_M \tag{13a}$$

where with $J, K = I, L, M$

$$\phi_J^K = \sum_{i=1}^{6}\hat{h}_i\phi_{Ji}^K \tag{13b}$$

in which h_I, h_L and h_M are the usual shape functions of the standard three-node linear triangular element, $\hat{h}_i$ is the standard shape function of the six-node triangular element, and ϕ_{Ji}^K ($J = I, L, M$) are given coefficients. We note that the ϕ_J^K correspond to weights on the usual interpolation functions h_I, h_L and h_M.

The nodal degrees of freedom $\mathbf{u}_J$ are in general given by

$$\mathbf{u}_J = p_n\mathbf{a}_{Jn} \tag{14}$$

in which the p_n are basis functions for the interpolation and the $\mathbf{a}_{Jn}$ are the nodal unknowns. For the "standard" linear overlapping elements, we use the p_n basis functions listed here in $\mathbf{p}$

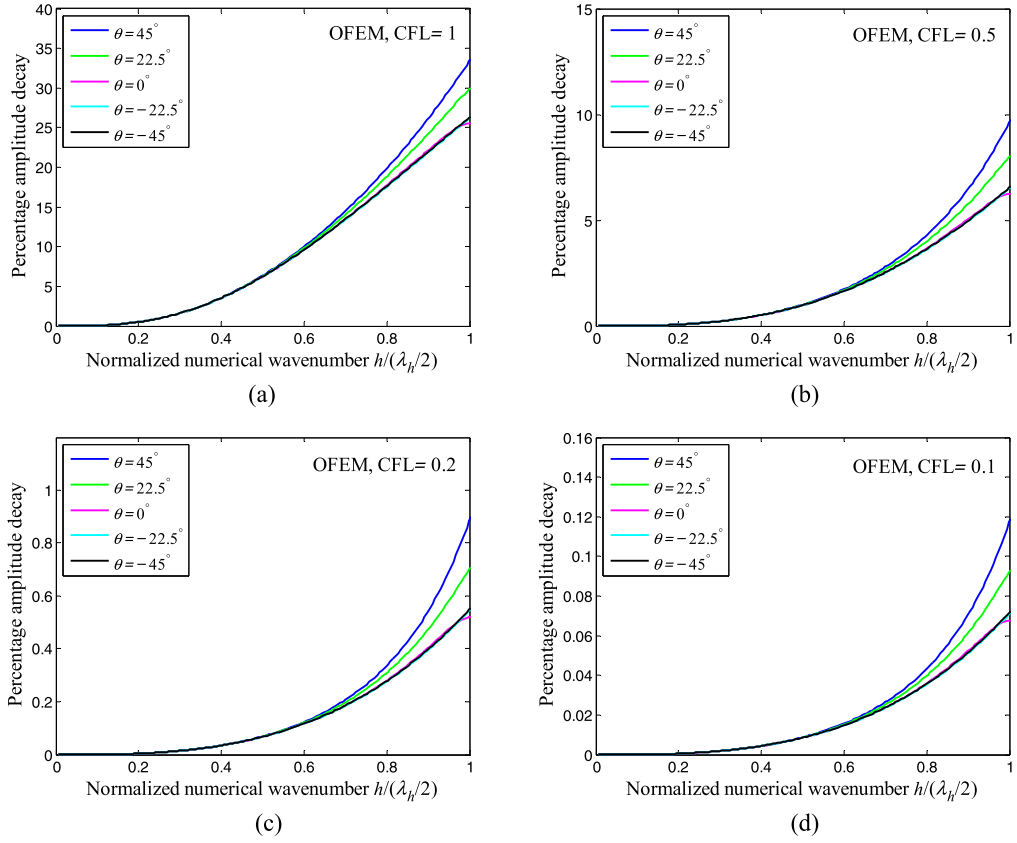

Fig. 8. Dissipation of the standard OFEM with Bathe time integration scheme: (a) CFL = 1; (b) CFL = 0.5; (c) CFL = 0.2; (d) CFL = 0.1.

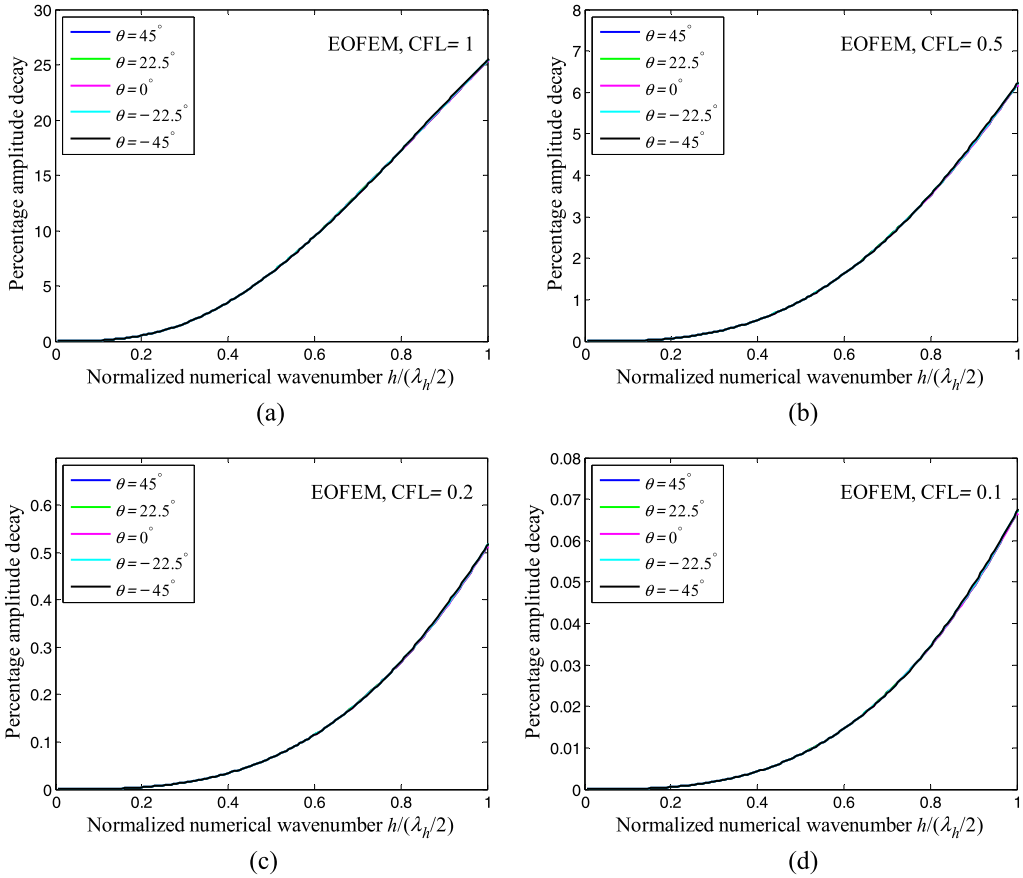

Fig. 9. Dissipation of the EOFEM with Bathe time integration scheme: (a) CFL = 1; (b) CFL = 0.5; (c) CFL = 0.2; (d) CFL=0.1.

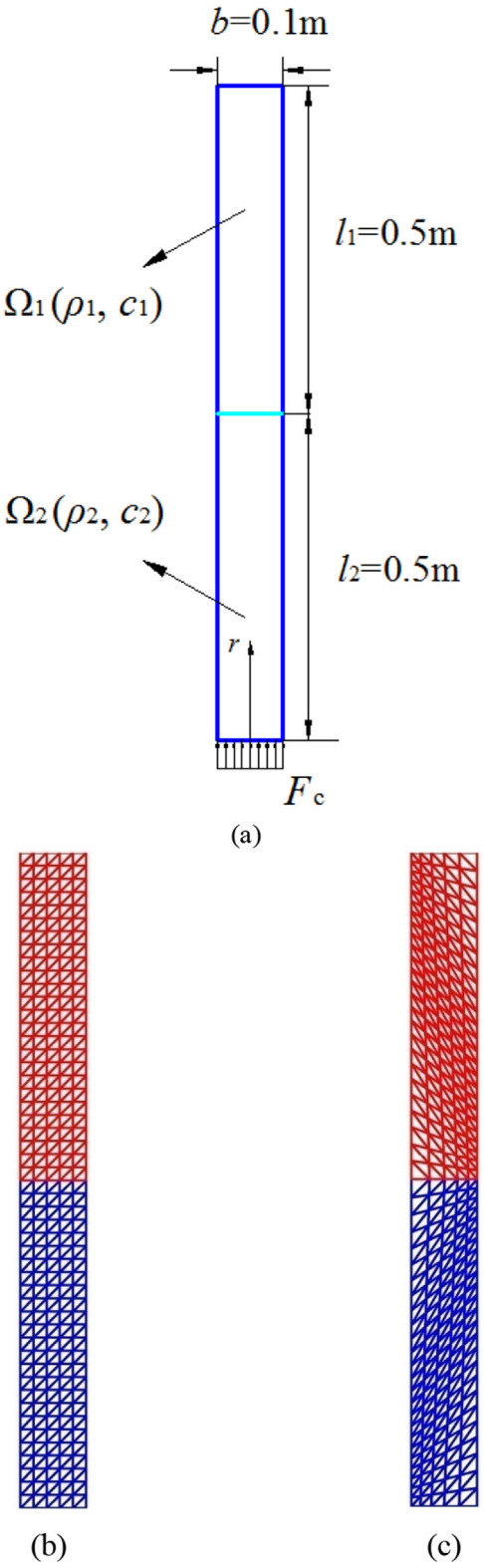

Fig. 10. Problem description and used meshes for the two-dimensional tube: (a) The tube; (b) The used uniform mesh; (c) The used distorted mesh.

$$\mathbf{p} = [1 \quad x \quad y] \tag{15}$$

However, for the solution of wave propagation problems we enrich the overlapping finite elements by trigonometric basis functions and use

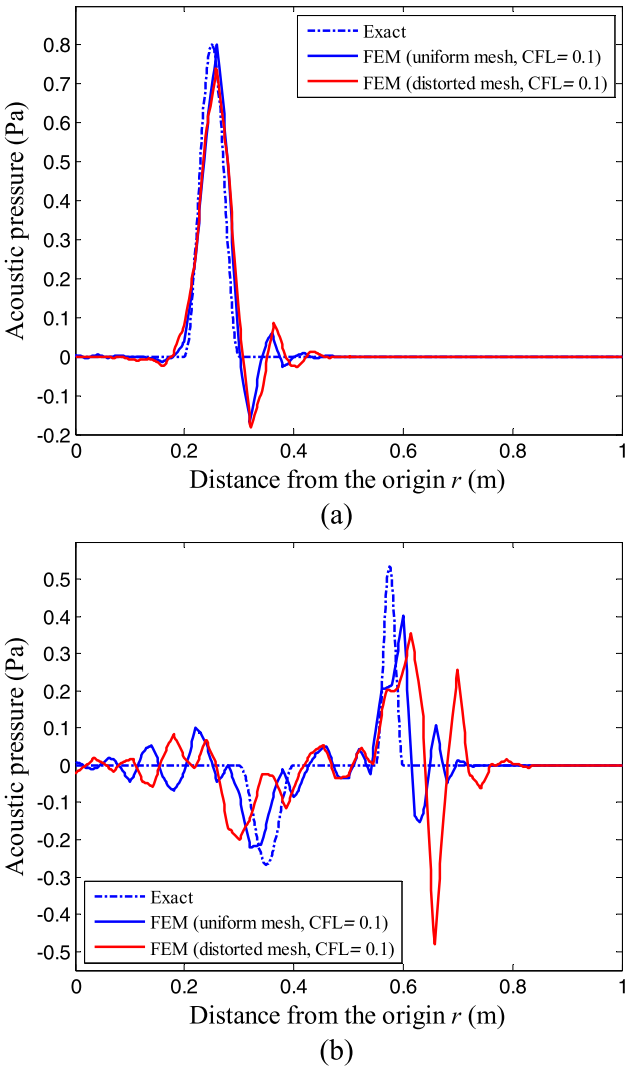

Fig. 11. The acoustic pressure predicted using the standard FEM at: (a) $t = 0.3$ s; (b) $t = 0.7$ s.

$$\mathbf{p} = \left\{ \begin{array}{l} 1, \quad x, \quad y, \\ \cos\left(\frac{2\pi x}{\lambda_x}\right), \quad \sin\left(\frac{2\pi x}{\lambda_x}\right), \quad \cos\left(\frac{2\pi y}{\lambda_y}\right), \quad \sin\left(\frac{2\pi y}{\lambda_y}\right), \\ \cos\left(\frac{2\pi x}{\lambda_x} + \frac{2\pi y}{\lambda_y}\right), \quad \sin\left(\frac{2\pi x}{\lambda_x} + \frac{2\pi y}{\lambda_y}\right), \\ \cos\left(\frac{2\pi x}{\lambda_x} - \frac{2\pi y}{\lambda_y}\right), \quad \sin\left(\frac{2\pi x}{\lambda_x} - \frac{2\pi y}{\lambda_y}\right), \\ \quad \cdots, \\ \cos\left(\frac{2\pi q x}{\lambda_x}\right), \quad \sin\left(\frac{2\pi q x}{\lambda_x}\right), \quad \cos\left(\frac{2\pi q y}{\lambda_y}\right), \quad \sin\left(\frac{2\pi q y}{\lambda_y}\right), \\ \cos\left(\frac{2\pi q x}{\lambda_x} + \frac{2\pi q y}{\lambda_y}\right), \quad \sin\left(\frac{2\pi q x}{\lambda_x} + \frac{2\pi q y}{\lambda_y}\right), \\ \cos\left(\frac{2\pi q x}{\lambda_x} - \frac{2\pi q y}{\lambda_y}\right), \quad \sin\left(\frac{2\pi q x}{\lambda_x} - \frac{2\pi q y}{\lambda_y}\right) \end{array} \right\} \tag{16}$$

In Eq. (16), (x, y) denotes the coordinate values in the Cartesian coordinate system, λ_x and λ_y are the fundamental wave lengths in the x- and y-directions, and q denotes the degree of the trigonometric function. A larger q provides more accurate numerical solutions, however this use may also lead to more computational cost for a given accuracy. In this paper we consider $q = 1$ and use $\lambda_x = \lambda_y = 2h$ in which h denotes the size of the overlapping element. Note that we do not include the term (xy) in Eq. (16) as was done in Ref. [14] because for the triangular element used this basis seems sufficient.

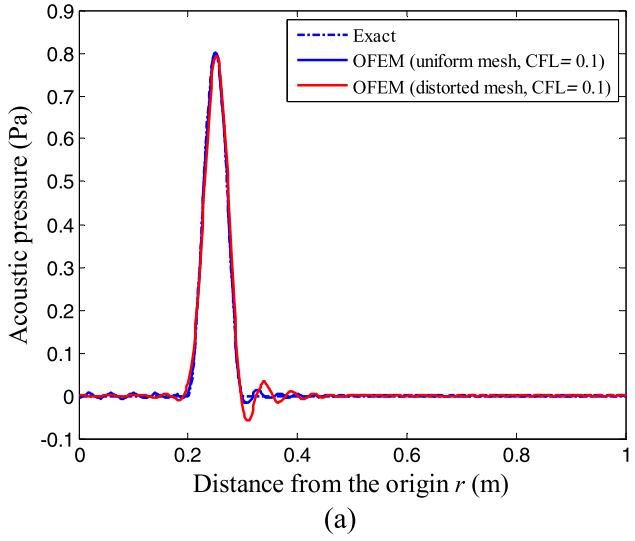

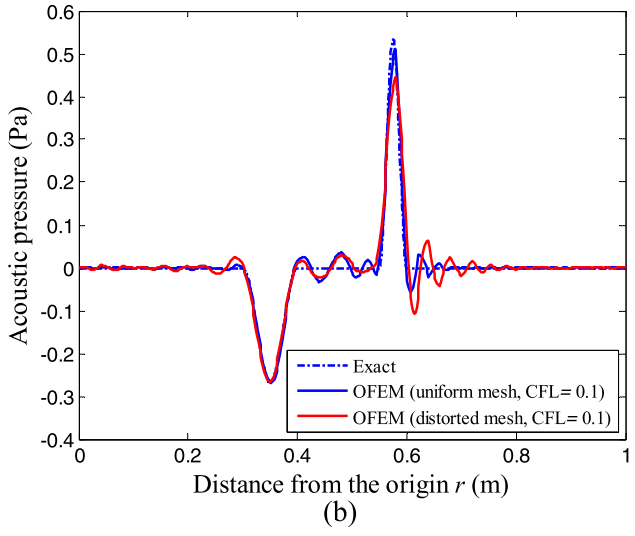

Fig. 12. The acoustic pressure predicted using the standard OFEM at: (a) $t = 0.3$ s; (b) $t = 0.7$ s.

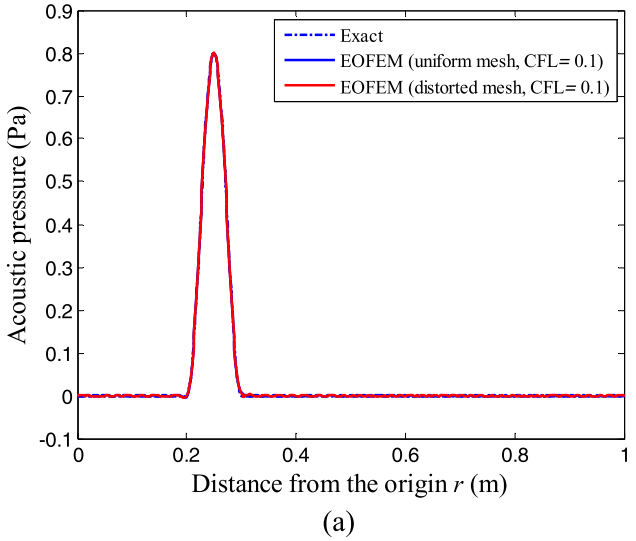

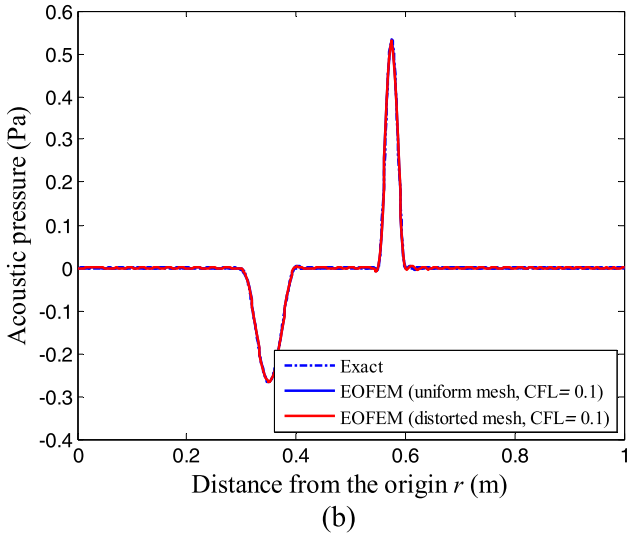

Fig. 13. The acoustic pressure predicted using the EOFEM at: (a) $t = 0.3$ s; (b) $t = 0.7$ s.

4. Dispersion analysis

The numerical solutions of wave propagation problems suffer from numerical dispersion errors. As a result, when using traditional finite element procedures, the solution accuracy in general becomes worse with an increase of the considered wave number, $k = \frac{2\pi}{\lambda}$, where λ is the (exact) wave length. Therefore, it is important to examine the dispersion properties of a numerical technique. In this section, we conduct a dispersion analysis using the uniform mesh in a homogeneous medium shown in Fig. 2: here θ is the angle between the wave propagation direction and the x-axis of the Cartesian coordinate system, and h is the nodal spacing of the mesh. We consider the errors due to the spatial discretization and the time integration. We use a homogeneous medium for the analysis because each of the subregions we consider are of constant material properties. The equations and results are based on Ref. [14] but we give now also novel insights.

To show the capabilities of the enriched overlapping triangular elements in solving wave propagations, we also give the numerical results when using the standard finite element method and when using the overlapping finite elements without including the harmonic functions (which was not done in Ref. [14]). For convenience of discussion, we use as abbreviations FEM, OFEM and EOFEM to denote the results using the standard linear triangular element, the "standard" overlapping finite element and the enriched overlapping finite element, respectively.

For the general wave equation in a homogeneous medium, also used in Eq. (1), a basic plane wave solution is given by

$$u = Ae^{i(k\mathbf{n}\cdot\mathbf{x}-\omega t)} \tag{17}$$

in which A is the amplitude of the wave, $\mathbf{n}$ is a unit vector into the wave propagation direction, $\mathbf{x}$ is the position vector of the considered point, t denotes time, k is the wave number given by $k = \omega/c$ and ω is the angular frequency.

4.1. Spatial discretization error

Eliminating the time dependency from the wave equation, the well-known Helmholtz equation is obtained

$$\nabla^2 u + k^2 u = 0 \tag{18}$$

for which the exact solution is, not considering boundary conditions,

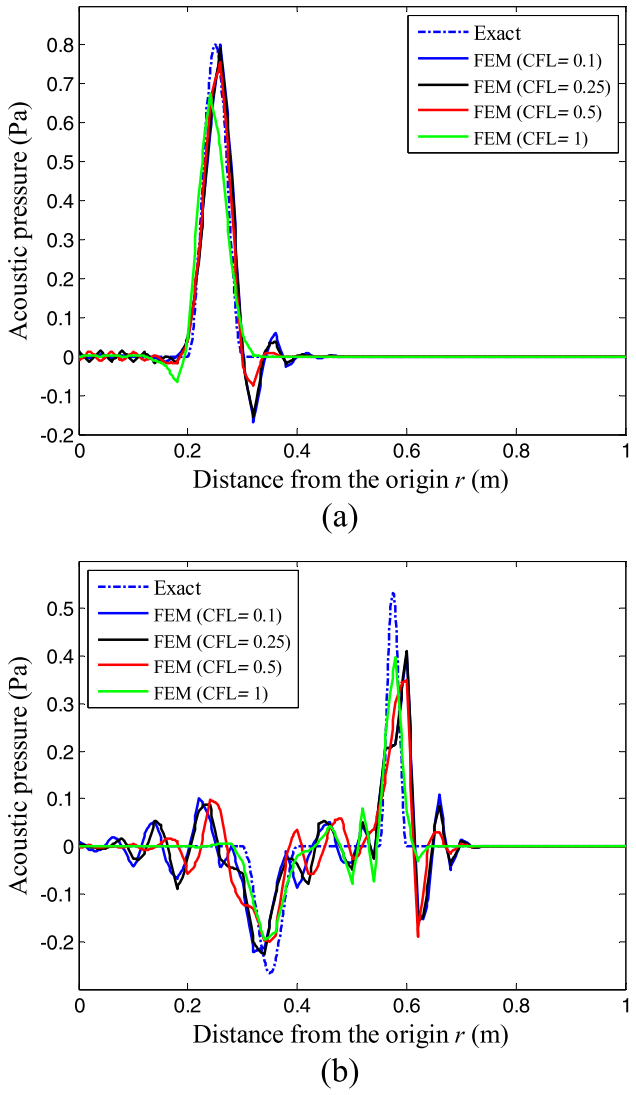

Fig. 14. The acoustic pressure predicted using the FEM, uniform mesh, with different CFL numbers: (a) $t = 0.3$ s; (b) $t = 0.7$ s.

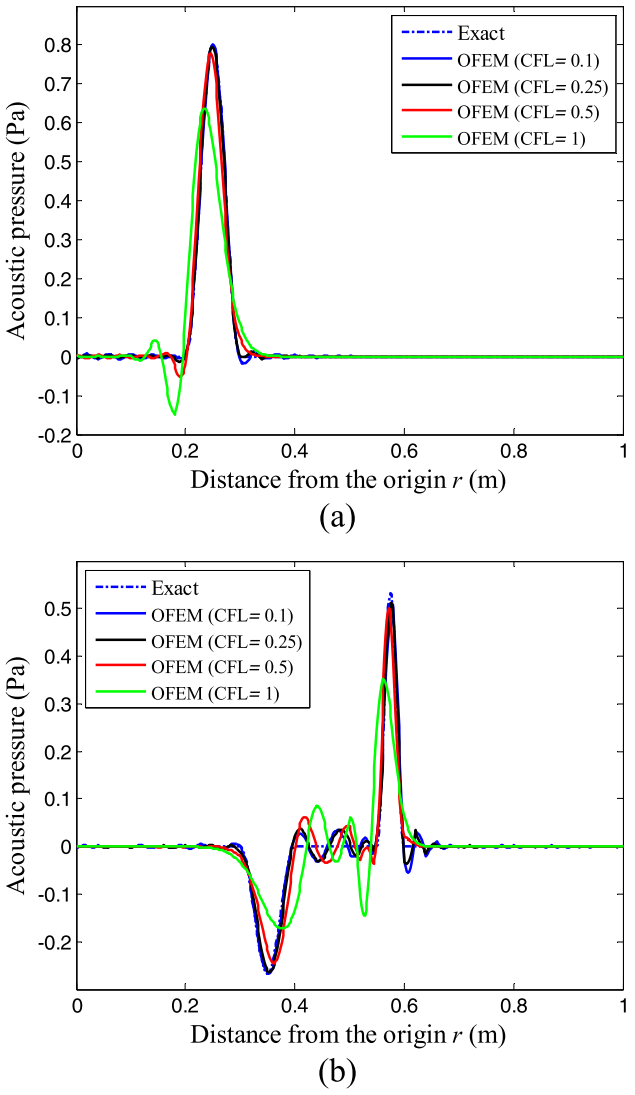

Fig. 15. The acoustic pressure predicted using the OFEM, uniform mesh, with different CFL numbers: (a) $t = 0.3$ s; (b) $t = 0.7$ s.

$$u = Ae^{ik\mathbf{n}\cdot\mathbf{x}} \tag{19}$$

Using the finite element interpolations given in Eq. (12) we have

$$\mathbf{Ka} - k^2\mathbf{Ma} = \mathbf{0} \tag{20}$$

in which $\mathbf{a}$ is the vector of unknown solution coefficients, $\mathbf{K}$ and $\mathbf{M}$ are the stiffness and mass matrices, respectively.

If we use the n_p local basis functions in Eq. (16), the solution vector has the following form

$$\mathbf{a} = \hat{\mathbf{a}}e^{ik_h\mathbf{n}\cdot\mathbf{x}} \tag{21}$$

in which k_h is the numerical wave number, and the amplitude vector $\hat{\mathbf{a}}$ is given by

$$\hat{\mathbf{a}} = \begin{bmatrix} A_1 & A_2 & \cdots & A_{n_p}, & A_1 & A_2 & \cdots & A_{n_p}, & \cdots \end{bmatrix}^T \tag{22}$$

with the A_j $(j = 1, 2, \cdots, n_p)$ corresponding to the local basis functions.

Since we consider a translationally invariant homogeneous mesh without a boundary condition, the local basis function solution for each node has identical amplitude, that is, the vector $\mathbf{a}_I = \begin{bmatrix} A_1 & A_2 & \cdots & A_{n_p} \end{bmatrix}^T$ for node I repeats itself for each node, as shown in Eq. (22).

Substituting Eq. (21) into Eq. (20) and removing the common factor, we obtain for a typical node

$$\left[\mathbf{D}_{\text{stiff}} - k^2\mathbf{D}_{\text{mass}}\right]\mathbf{a}_I = \mathbf{0} \tag{23}$$

in which $\mathbf{D}_{\text{stiff}}$ and $\mathbf{D}_{\text{mass}}$ are Hermitian matrices corresponding to the stiffness matrix $\mathbf{K}$ and mass matrix $\mathbf{M}$, respectively.

The dimension of $\mathbf{D}_{\text{stiff}}$ and $\mathbf{D}_{\text{mass}}$ is $n_p \times n_p$, and referring to Fig. 2,

$$\begin{aligned}\mathbf{D}_{\text{stiff}} = {} & \mathbf{K}_{n,n} + \mathbf{K}_{n,n-1}e^{-ik_h h\cos\theta} + \mathbf{K}_{n,n+1}e^{ik_h h\cos\theta} + \\ & \mathbf{K}_{n,n-2}e^{ik_h h(\cos\theta-\sin\theta)} + \mathbf{K}_{n,n+2}e^{ik_h h(-\cos\theta+\sin\theta)} + \\ & \mathbf{K}_{n,n-3}e^{-ik_h h\sin\theta} + \mathbf{K}_{n,n+3}e^{ik_h h\sin\theta} + \\ & \mathbf{K}_{n,n-4}e^{ik_h h(-\cos\theta-\sin\theta)} + \mathbf{K}_{n,n+4}e^{ik_h h(\cos\theta+\sin\theta)}\end{aligned} \tag{24}$$

$$\begin{aligned}\mathbf{D}_{\text{mass}} = {} & \mathbf{M}_{n,n} + \mathbf{M}_{n,n-1}e^{-ik_h h\cos\theta} + \mathbf{M}_{n,n+1}e^{ik_h h\cos\theta} + \\ & \mathbf{M}_{n,n-2}e^{ik_h h(\cos\theta-\sin\theta)} + \mathbf{M}_{n,n+2}e^{ik_h h(-\cos\theta+\sin\theta)} + \\ & \mathbf{M}_{n,n-3}e^{-ik_h h\sin\theta} + \mathbf{M}_{n,n+3}e^{ik_h h\sin\theta} + \\ & \mathbf{M}_{n,n-4}e^{ik_h h(-\cos\theta-\sin\theta)} + \mathbf{M}_{n,n+4}e^{ik_h h(\cos\theta+\sin\theta)}\end{aligned} \tag{25}$$

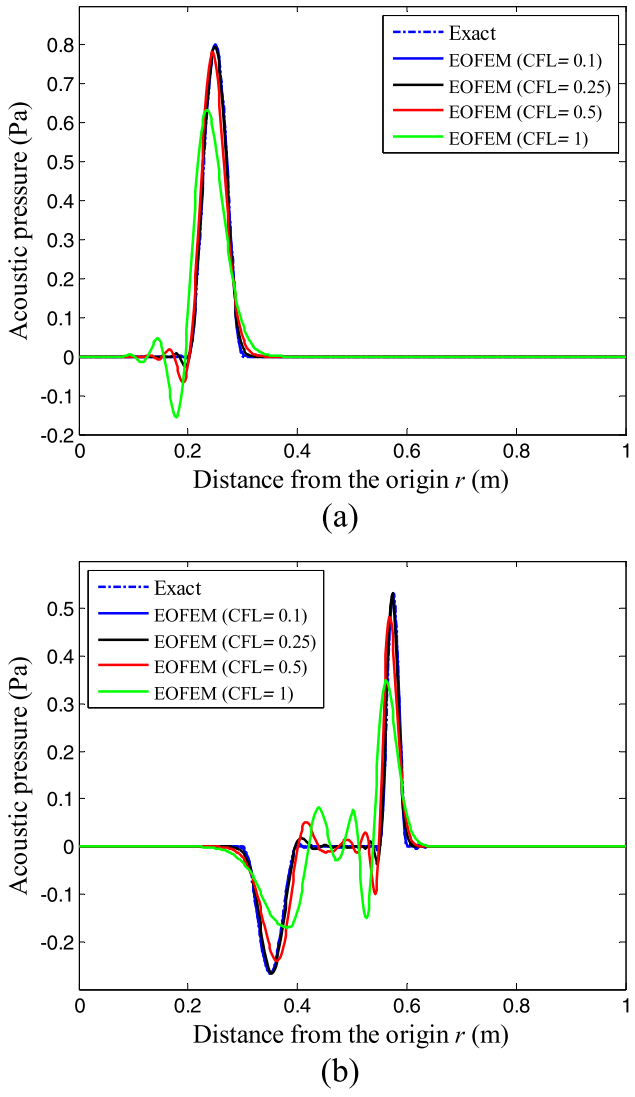

Fig. 16. The acoustic pressure predicted using the EOFEM, uniform mesh, with different CFL numbers: (a) $t = 0.3$ s; (b) $t = 0.7$ s.

For a non-trivial solution of Eq. (23) we must have

$$\det\left[\mathbf{D}_{\text{stiff}} - k^2\mathbf{D}_{\text{mass}}\right] = 0 \tag{26}$$

and we can obtain for any given numerical wave number k_h the corresponding exact wave number k.

The numerical wave number k_h is in general different from the exact wave number k due to dispersion error. We use the measure k/k_h to quantify the dispersion error induced by the spatial discretization.

The dispersion properties of the standard finite element method (FEM), the overlapping finite element discretization (OFEM) and the proposed enriched overlapping finite element method (EOFEM) are given in Fig. 3 as a function of $h/(\lambda_h/2)$ (=$k_h h/\pi$), where λ_h is the numerical wavelength. The results show that the dispersion error of the OFEM is clearly smaller than the error obtained using the FEM, but the proposed EOFEM performs best, indeed its dispersion error is almost zero for $h/(\lambda_h/2) < 1$. In addition, we also find that the dispersion properties of the FEM are strongly influenced by the direction of wave propagation. This numerical anisotropy is relieved to some extent using the OFEM and is almost completely removed in the EOFEM. These observations indicate that the EOFEM behaves much better in reducing numerical dispersion arising from the spatial discretizations and can provide more accurate solutions than using the standard FEM and OFEM (and referring to Ref. [14] the enriched finite element method). The reasons are the use of the overlapping finite elements and the use of harmonic functions in the formulation of the EOFEM.

4.2. Temporal discretization error

The numerical solutions of transient wave propagation problems also suffer from a temporal discretization error due to the time integration method used. Here we investigate the temporal discretization error of the EOFEM when using the standard Bathe time integration scheme [26,27].

Using the interpolation shown in Eq. (12) to solve the general wave equation, we obtain

$$\mathbf{M}\ddot{\mathbf{a}} + c^2\mathbf{K}\mathbf{a} = \mathbf{0} \tag{27}$$

where

$$\mathbf{a} = \hat{\mathbf{a}}e^{i(k_h\mathbf{n}\cdot\mathbf{x}-\omega_h t)} \tag{28}$$

in which k_h, ω_h and t are the numerical wave number, angular frequency and time, which is given by the number of time steps used.

With Eq. (28), Eq. (27) can be re-written as

$$\mathbf{D}_{\text{mass}}\ddot{\tilde{\mathbf{a}}} + c^2\mathbf{D}_{\text{stiff}}\tilde{\mathbf{a}} = 0 \tag{29}$$

where $\tilde{\mathbf{a}}$ is a function of time.

Diagonalizing Eq. (29) by its natural modes and using the standard Bathe time integration scheme, with two equal sub-steps per time step, the following discretized wave equation over two time steps can be obtained for a wave mode, see Ref. [14] for the detailed derivation

$${}^{t+2\Delta t}x + p^{t+\Delta t}x + q^t x = 0 \tag{30}$$

where $p = -\frac{288-94\omega^2\Delta t^2}{144+25\omega^2\Delta t^2+\omega^4\Delta t^4}$ and $q = \frac{144+25\omega^2\Delta t^2}{144+25\omega^2\Delta t^2+\omega^4\Delta t^4}$, with $\omega = kc$ the angular frequency of the wave mode obtained from Eq. (26) for a given k_h.

Using the time dependency in Eq. (28) in Eq. (30), we have

$$\left(e^{-i\omega_h\Delta t}\right)^2 + pe^{-i\omega_h\Delta t} + q = 0 \tag{31}$$

From Eq. (31), the numerical angular frequency ω_h is obtained and then the total dispersion error denoted by the normalized numerical phase velocity can be calculated using

$$\frac{c_h}{c} = \frac{\omega_h/k_h}{c} \tag{32}$$

Note that there are two complex conjugate roots for Eq. (31), hence the discrete solution to Eq. (30) has the following form

$$a_h = \gamma_1 e^{(-\xi_h+i)\omega_h\Delta t} + \gamma_2 e^{(-\xi_h-i)\omega_h\Delta t} \tag{33}$$

in which ξ_h is the numerical damping ratio, γ_1 and γ_2 are two undetermined coefficients.

From Eqs. (31) and (33), the following equations can be obtained

$$\omega_h\Delta t = \begin{cases} \arctan\left(-\frac{\sqrt{4q-p^2}}{p}\right), & \text{for } \Delta t < \Delta t^* \\ \arctan\left(\frac{\sqrt{4q-p^2}}{p}\right), & \text{for } \Delta t > \Delta t^* \end{cases} \tag{34a}$$

$$\xi_h = -\frac{1}{2}\frac{\ln(q)}{\omega_h\Delta t} \tag{34b}$$

in which $(4q-p^2)\big|_{\Delta t=\Delta t^*} = 0$ and the percentage amplitude decay (AD) is given by

$$\text{AD} = \left(1 - e^{-2\pi\xi_h}\right) \times 100\% \tag{35}$$

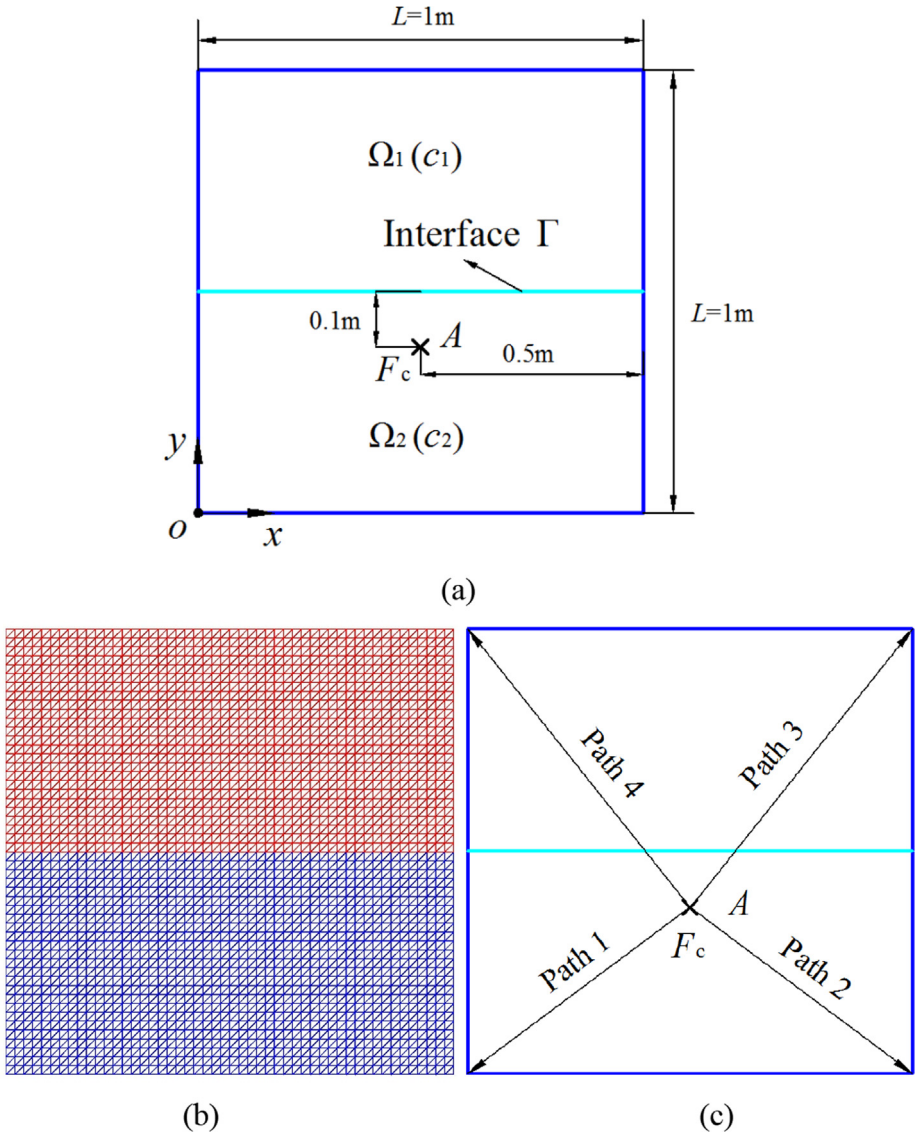

Fig. 17. The square pre-stressed membrane of different media: (a) Geometry description of the considered square domain; (b) The used uniform mesh; (c) The pre-defined paths.

Using Eq. (30), we find that the parameters p and q are functions of $\omega\Delta t$, so the solution (namely $\omega_h\Delta t$) to Eq. (31) is also a function of $\omega\Delta t$ and can be expressed as

$$\omega_h\Delta t = f(\omega\Delta t) \tag{36}$$

and note that

$$\omega\Delta t = kh\frac{c\Delta t}{h} = kh\,\mathrm{CFL} \tag{37}$$

in which $\mathrm{CFL} = c\Delta t/h$ with h (as defined above already) being the size of the overlapping element.

Hence Eq. (32) can be re-written as

$$\frac{c_h}{c} = \frac{\omega_h/k_h}{c} = \frac{\omega_h\Delta t}{k_h c\Delta t} = \frac{\omega_h\Delta t}{k_h h\mathrm{CFL}} = \frac{f(\omega\Delta t)}{k_h h\mathrm{CFL}} = \frac{f(kh\mathrm{CFL})}{k_h h\mathrm{CFL}} \tag{38}$$

For a small CFL number we have

$$\begin{aligned} f(\omega\Delta t) &= \arctan\left(\omega\Delta t\frac{144-5\omega^2\Delta t^2}{144-47\omega^2\Delta t^2}\right) \\ &= \arctan\left[kh\,\mathrm{CFL}\frac{144-5(kh\,\mathrm{CFL})^2}{144-47(kh\,\mathrm{CFL})^2}\right] \end{aligned} \tag{39}$$

Using the Taylor series expansion, we obtain

$$\begin{aligned} \left(\tfrac{c_h}{c}\right)_{\mathrm{BM}} &= \tfrac{1}{k_h h\mathrm{CFL}}\left[f(0)+f'(0)(kh\mathrm{CFL})+\tfrac{f''(0)}{2!}(kh\mathrm{CFL})^2+\cdots\right] \\ &= \tfrac{k}{k_h}\underbrace{\left[1-\frac{1}{24}(kh\mathrm{CFL})^2+\frac{61}{17280}(kh\mathrm{CFL})^4+\cdots\right]}_{\text{Temporal discretization error}} \end{aligned} \tag{40}$$

As a side result, using similar steps, we can obtain for the trapezoidal rule [26] a similar expression

$$\left(\frac{c_h}{c}\right)_{\mathrm{TR}} = \frac{k}{k_h}\underbrace{\left(1-\frac{1}{12}(kh\mathrm{CFL})^2+\frac{1}{80}(kh\mathrm{CFL})^4+\cdots\right)}_{\text{Temporal discretization error}} \tag{41}$$

We note that Eq. (32) can also be written as

$$\frac{c_h}{c} = \frac{\omega_h/k_h}{\omega/k} = \frac{k}{k_h}\frac{\omega_h}{\omega} = \frac{k}{k_h}\frac{T}{T_h} \tag{42}$$

in which T and T_h are the exact and numerical period of the wave mode, respectively.

Eqs. (40)–(42) show that the total wave speed error c_h/c can be split into two different parts: the first part (namely k/k_h) is the

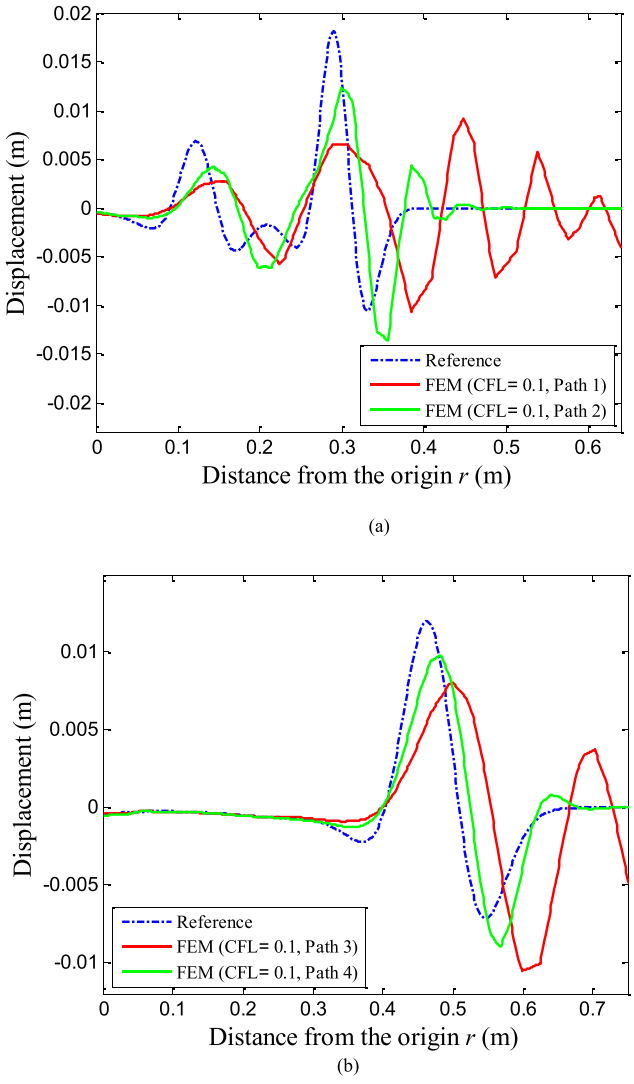

Fig. 18. Comparisons of the displacement solutions using the FEM at $t = 0.4$ s: (a) Path 1 and Path 2; (b) Path 3 and Path 4.

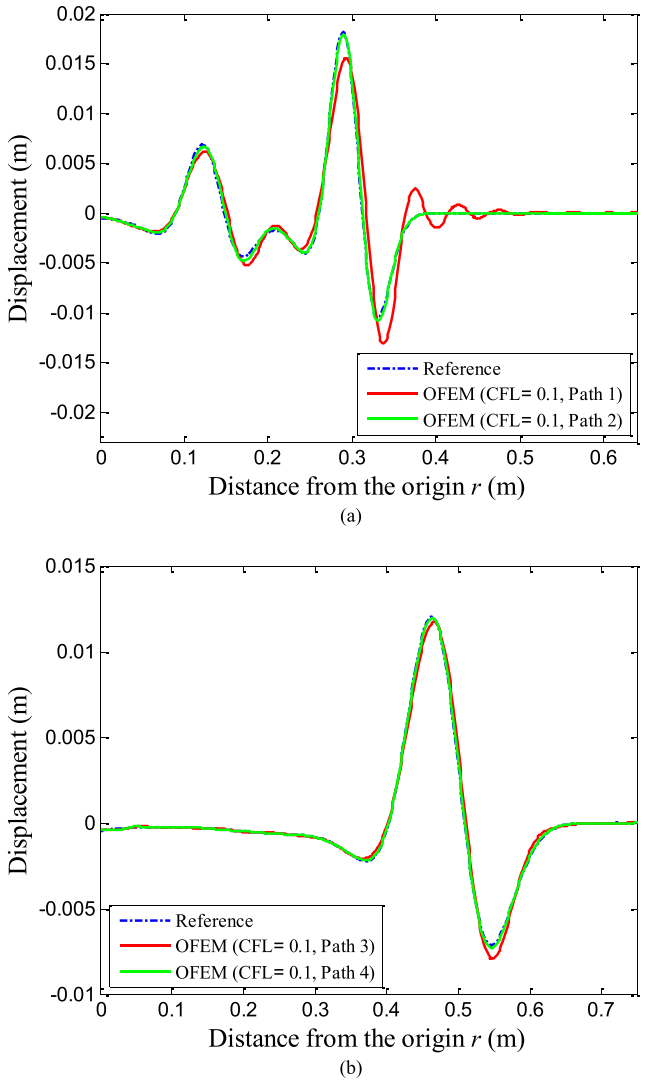

Fig. 19. Comparisons of the displacement solutions using the standard OFEM at $t = 0.4$ s: (a) Path 1 and Path 2; (b) Path 3 and Path 4.

numerical error due to the spatial discretization and the second part is the numerical error due to the temporal discretization. The spatial dispersion error depends only on the spatial discretization (that is, the spatial interpolation and mesh used) while the temporal dispersion error is only related to the temporal discretization (that is, the time integration scheme and time step used). For a given mesh pattern, the spatial dispersion error k/k_h can be determined by Eq. (26), while the temporal dispersion error tends to zero by decreasing the time step (that is, as CFL $\rightarrow$ 0). Hence, the total wave speed error c_h/c converges to the spatial discretization error k/k_h as CFL $\rightarrow$ 0.

We also note from Eq. (40) that the function of the temporal error $f(kh\text{CFL})$ is a monotonic function with respect to khCFL, hence the total wave speed error c_h/c converges *monotonically* to the spatial discretization error k/k_h as the time step tends to zero. Since the spatial dispersion error of the EOFEM is almost zero in all directions when the normalized numerical wavenumber $k_h h/\pi < 1$ (see Fig. 3), the accuracy of the numerical solutions using the EOFEM is monotonically improved by using a smaller CFL. The same conclusion also holds for the trapezoidal rule, which however, shows other significant disadvantages [7,28].

Figs. 4–6 give the total dispersion error using the standard FEM, standard OFEM and the present EOFEM for different CFL numbers. We see that, indeed, the total wave speed error c_h/c converges monotonically to the spatial discretization error k/k_h as the CFL number decreases. This is an important property for the solution of wave propagation problems in practical analysis because, firstly, the accuracy of the numerical solution of a single wave (traveling at one wave speed) is increased by simply refining the mesh and decreasing the time step, and secondly, this monotonic increase in accuracy also holds when multiple waves with different speeds are calculated in the solution of complex wave propagation problems.

Figs. 7–9 give the dissipation properties of the three mentioned methods as a function of the CFL numbers used. We see that the amplitude decay using any of the methods decreases as a smaller CFL number is used, however, the amplitude decay using the EOFEM is smallest, has the desired monotonic increase with wave number, and, importantly, is almost insensitive to the direction of wave propagation.

5. Numerical examples

In the previous section, we examined the dispersion and dissipation properties of the EOFEM in the solution of wave propagation

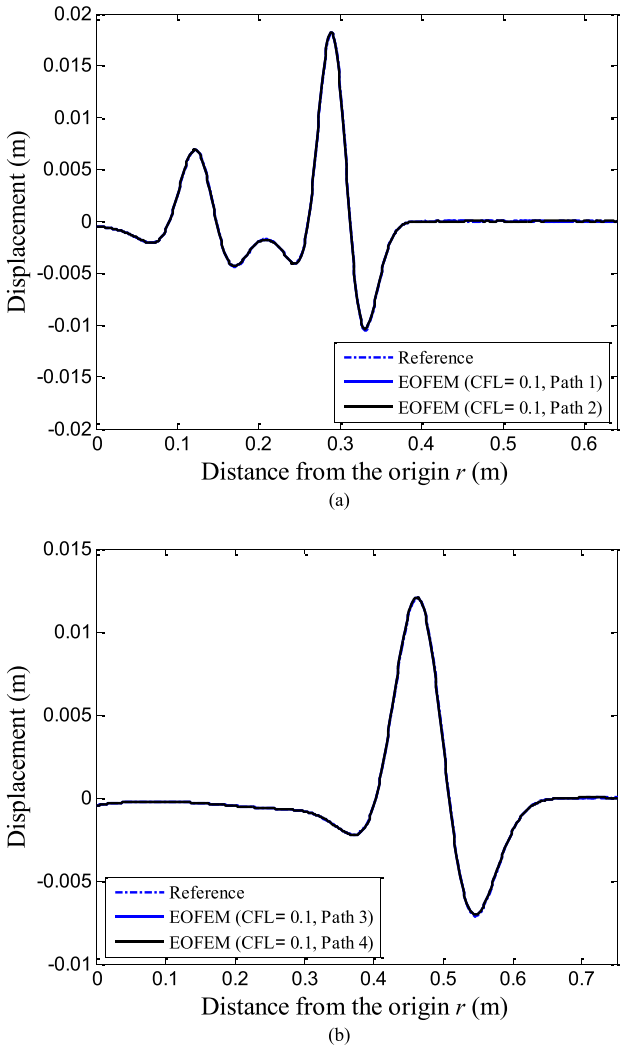

Fig. 20. Comparisons of the displacement solutions using the EOFEM at $t = 0.4$ s: (a) Path 1 and Path 2; (b) Path 3 and Path 4.

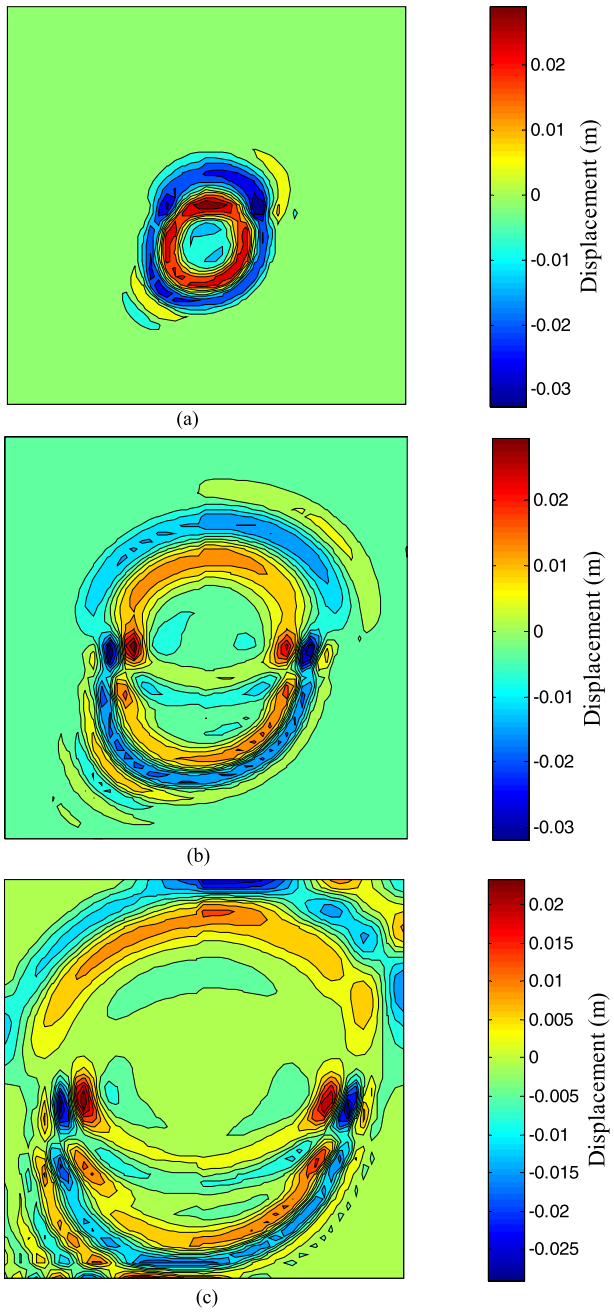

Fig. 21. Snapshots of the displacement distributions using the FEM at: (a) $t = 0.2$ s; (b) $t = 0.3$ s; (c) $t = 0.4$ s.

problems. Although the investigation was based on using a uniform mesh pattern, the conclusions have significance for solving wave propagation problems for which non-uniform meshes need generally be used.

In this section, we solve several wave propagation problems to illustrate the performance of the EOFEM with the Bathe time integration scheme. We consider wave propagations in inhomogeneous media with reflected and transmitted waves and compare the predictive capabilities with those of the standard FEM and OFEM. In all analyses we use the triangular elements discussed above and fixed reasonable meshes, that is, we do not include a study of using different meshes and element sizes. Also, in all cases, the solution times considered are such that the waves do not reach the boundary of the problem domain, hence non-reflecting boundary conditions are not used in the models.

5.1. Pressure waves traveling in a tube

We consider a two-dimensional tube of length 1 m and width 0.1 m. As shown in Fig. 10a, the tube is filled with two different acoustic fluid media (ρ is the density of the fluid medium and c is the wave speed). The physical parameters of the two fluid media are $\rho_1 = \rho_2$, $c_1 = 0.5$ m/s and $c_2 = 1$ m/s. The interface is located at $r = 0.5$ m. An excitation pressure $u = 0.8\sin(20\pi t)$, $t \in [0,\ 0.05]$ is imposed at the bottom of the tube. We impose slip boundary conditions along the vertical walls, hence in essence we have a one-dimensional wave propagation problem and the analytical solution can be readily obtained. For the numerical solutions we use uniform and distorted meshes (see Fig. 10b and c) with a mesh of $2 \times 5 \times 50$ triangular elements. For the distorted mesh we use the same characteristic element length h as for the undistorted mesh, $h = 0.02$ m, and for the CFL number we use $c = 1$ m/s.

Fig. 11 gives acoustic pressure results for times $t = 0.3$ s and $t = 0.7$ s obtained using the standard FEM and CFL = 0.1. In Fig. 11b, the small peak corresponds to the reflected wave while

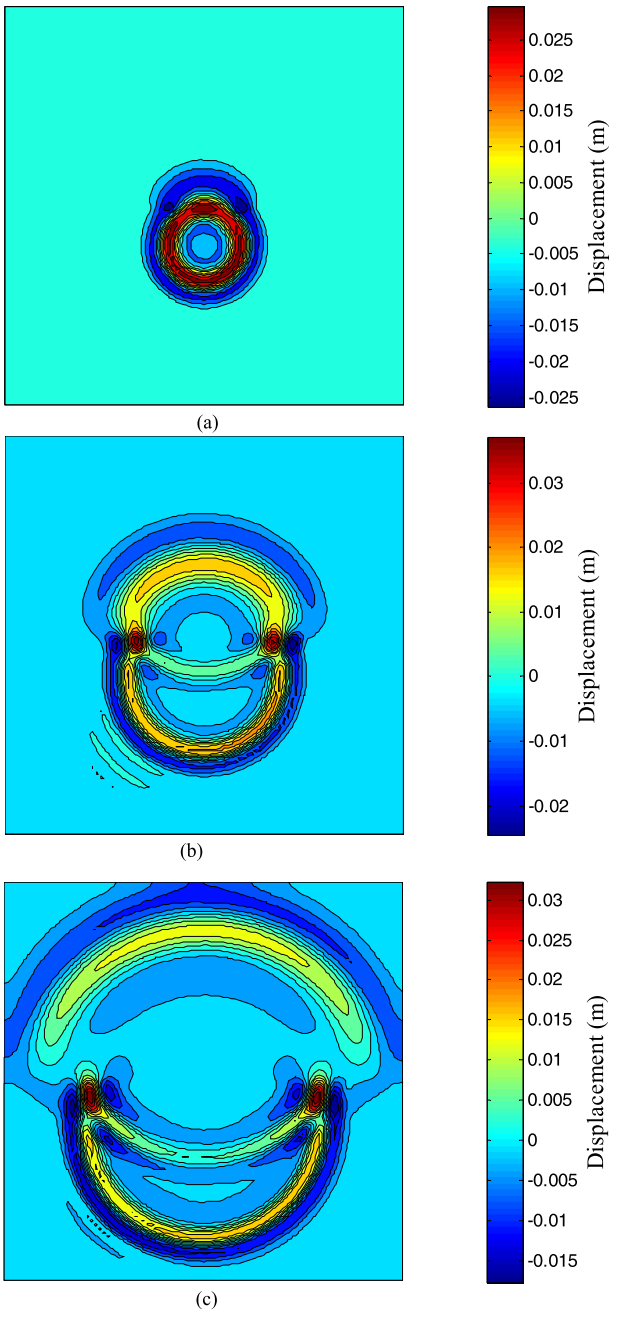

Fig. 22. Snapshots of the displacement distributions using the OFEM at: (a) $t = 0.2$ s; (b) $t = 0.3$ s; (c) $t = 0.4$ s.

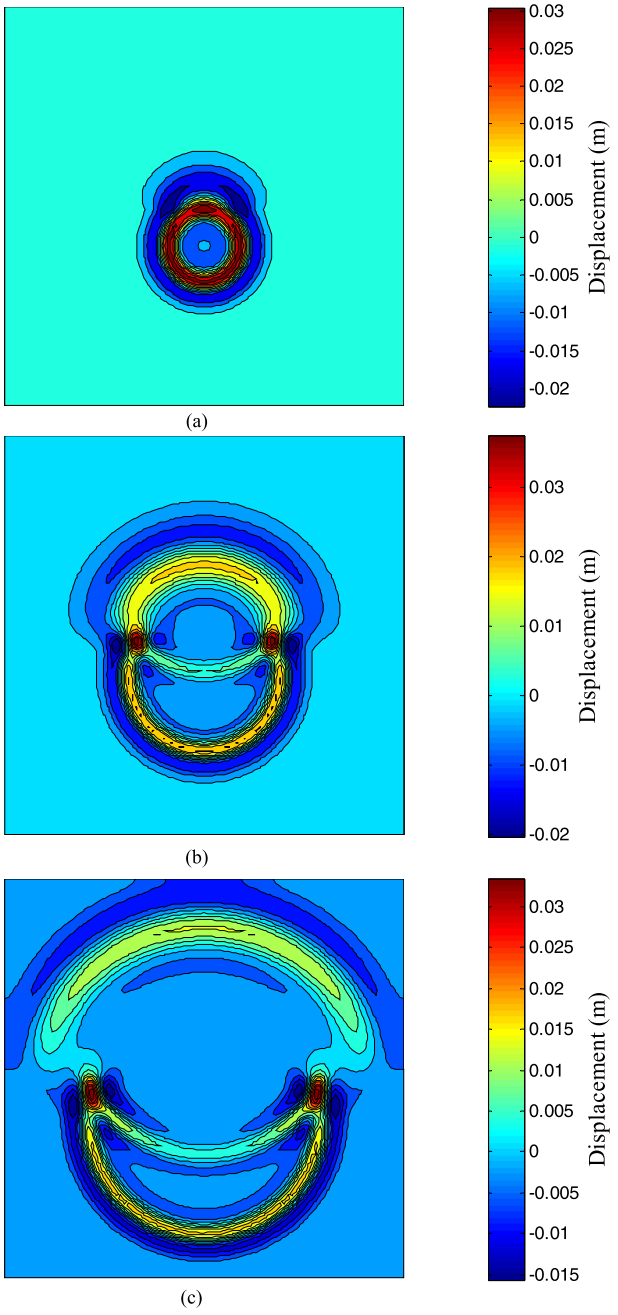

Fig. 23. Snapshots of the displacement distributions using the EOFEM at: (a) $t = 0.2$ s; (b) $t = 0.3$ s; (c) $t = 0.4$ s.

the large peak corresponds to the transmitted wave through the interface. We see that the computed results are not accurate, but the results using the uniform mesh are slightly better than those employing the distorted mesh. The corresponding results using the OFEM and EOFEM are presented in Figs. 12 and 13. The results using the OFEM are better than the FEM results but the EOFEM results are best and agree well with the exact solution. We also note that the EOFEM results are almost unchanged if instead of the uniform mesh we use the distorted mesh.

To investigate the monotonic convergence property, we use different CFL numbers and obtain the results shown in Figs. 14–16. We see that for the given meshes the EOFEM results can be improved by using a smaller CFL number while this property does not hold for the standard FEM and only somewhat for the OFEM. As mentioned earlier, the monotonic convergence of the solution (as the mesh is refined and the CFL decreases) is an important property because it renders the EOFEM very suitable for solving transient wave propagation problems in inhomogeneous media containing different types of waves traveling at different speeds.

5.2. A two-dimensional square domain with inhomogeneous media

Fig. 17a shows the 2D problem considered: a square prestressed membrane (length $L = 1$ m) of two different media. The wave speed in the two different media are $c_1 = 2$ m/s and $c_2 = 1$ m/s, and the interface is at $y = 0.5$ m. A uniform triangular mesh of $2 \times 50 \times 50$ elements is employed to discretize the prob-

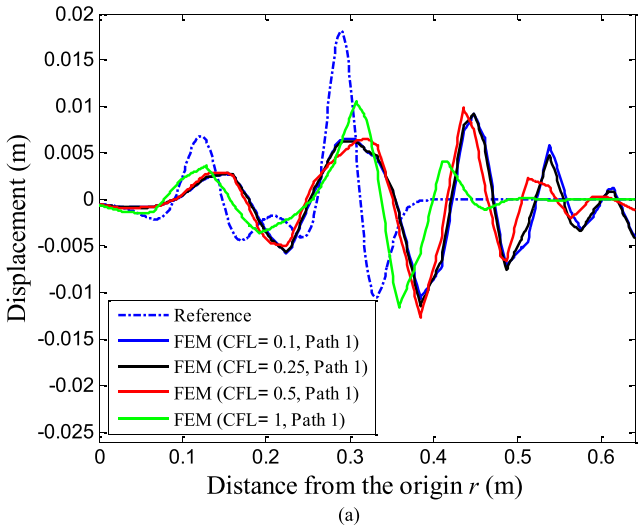

Fig. 24. The displacement predicted using the FEM with different CFL numbers at $t = 0.4$ s: (a) Path 1; (b) Path 3.

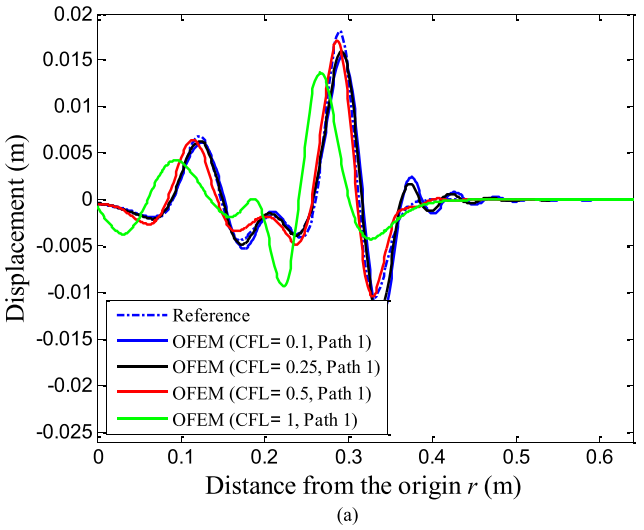

Fig. 25. The displacement predicted using the OFEM with different CFL numbers at $t = 0.4$ s: (a) Path 1; (b) Path 3.

lem domain (see Fig. 17b). A concentrated Ricker wavelet force F_c is imposed at point A

$$F_c = 0.4\left[1 - 2\pi^2 f_p^2 (t - t_s)^2\right]\exp\left(-\pi^2 f_p^2 (t - t_s)^2\right) \tag{43}$$

with the peak frequency $f_p = 10$ Hz and the time shift $t_s = 0.1$ s. For the CFL number we use $h = 0.02$ m and $c = 1$ m/s.

To compare computed results we focus on the paths shown in Fig. 17c. The predicted displacement solutions at $t = 0.4$ s and using CFL = 0.1 with the three methods are plotted in Figs. 18–20. The results include a reference solution obtained with a very fine mesh using the EOFEM with CFL = 0.1. The high peak is the original wave from the source and the lower peak corresponds to the wave reflected by the interface of the two different media.

We see that the results using the EOFEM are much better than the results obtained with standard FEM and are also better than those using the OFEM.

Figs. 21–23 present several snapshots of the displacement distributions obtained using the three methods at different observation times. It is clearly seen that the EOFEM solutions are smoother and better than those obtained with the standard FEM and OFEM solutions.

Finally, we examine the convergence of the three methods as a function of the CFL number. The results are given in Figs. 24–26. We see again that the EOFEM shows monotonic convergence in the solution of the problem while the standard FEM and OFEM do not display this property.

5.3. Two-dimensional acoustic wave scattering by a circular object

Next we consider the acoustic wave propagation in a square pre-stressed membrane containing four circular regions; the exterior and interior domains of the circular regions are of different media, see Fig. 27. The wave source is at the center of the square domain and the concentrated excitation force is a Ricker wavelet of magnitude 0.4, peak frequency $f_p = 10$ Hz and time shift $t_s = 0.1$ s. Due to symmetry, only the domain $[0, 1] \times [0, 1]$ is modelled in the analysis. The wave speeds in the two considered media are $c_1 = 2$ m/s and $c_2 = 1$ m/s. Along each side of the square domain 40 triangular elements are used with element size $h = 0.025$ m. To compare the numerical solutions, we use the three lines shown in

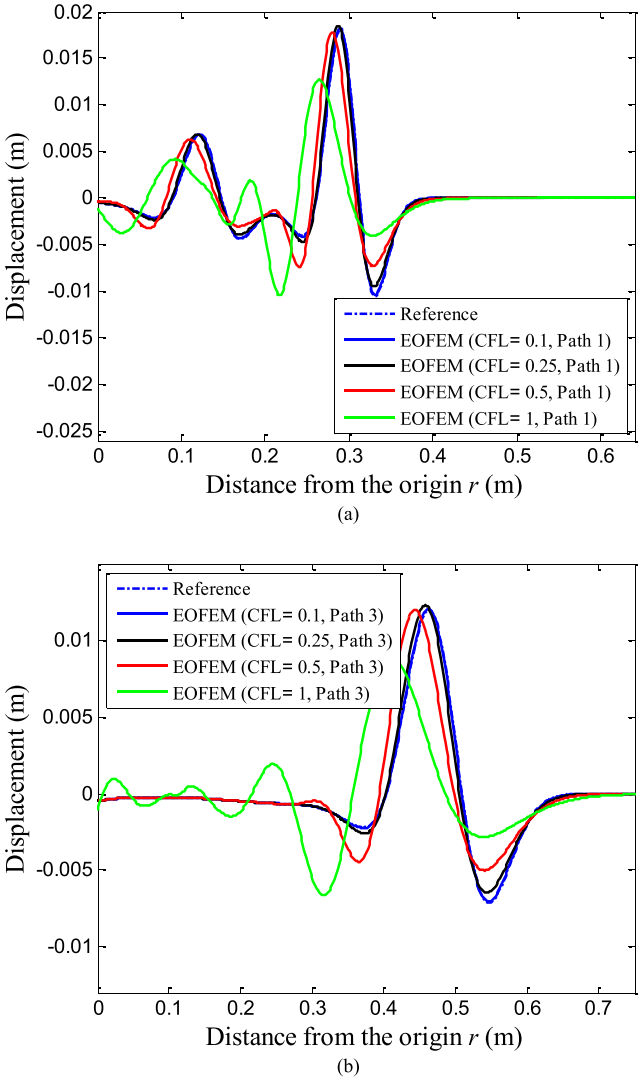

Fig. 26. The displacement predicted using the EOFEM with different CFL numbers at $t = 0.4$ s: (a) Path 1; (b) Path 3.

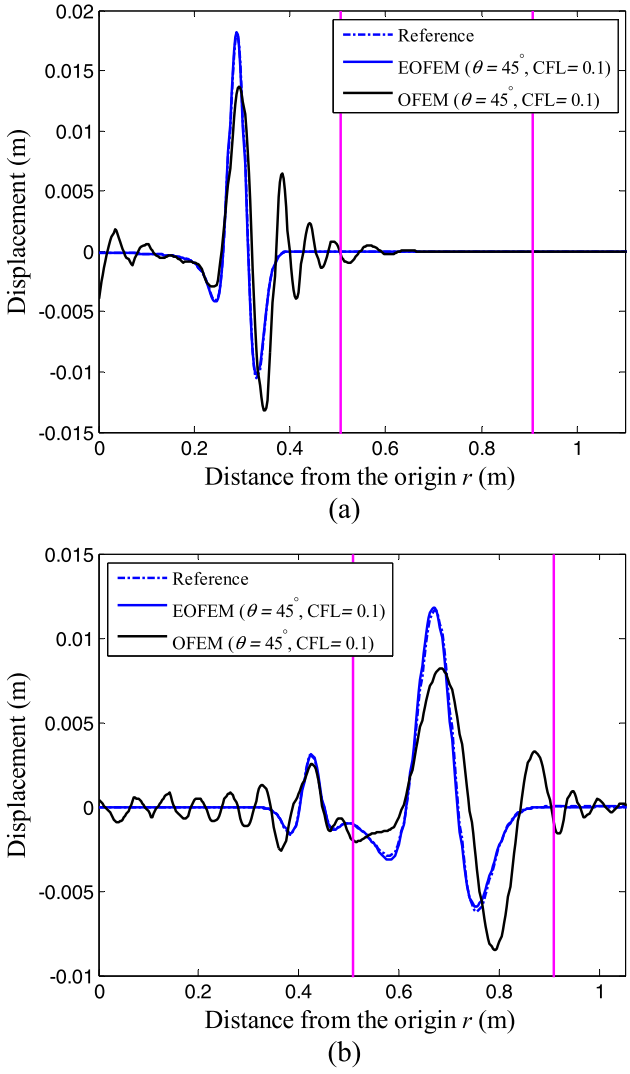

Fig. 28. The displacement solutions of the two-dimensional scalar wave scattering problem using OFEM and EOFEM at observation times: (a) $t = 0.4$ s; (b) $t = 0.7$ s.

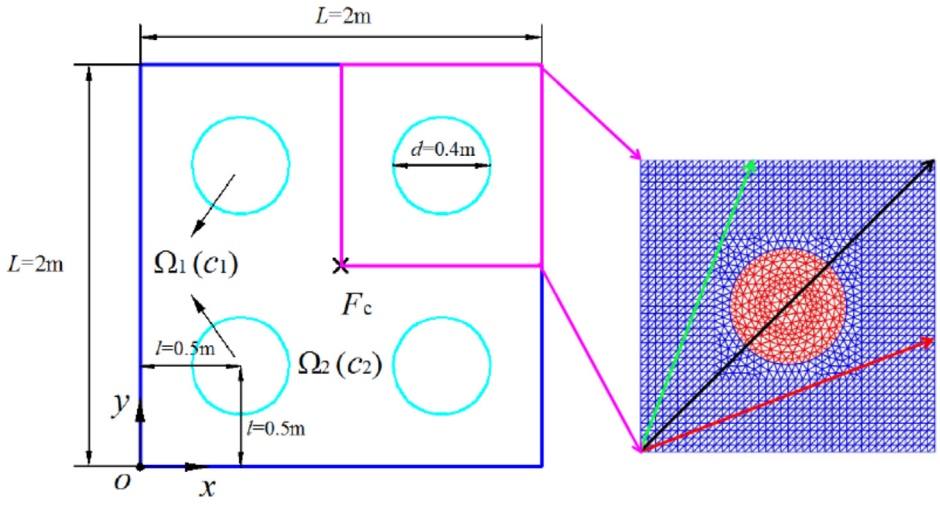

Fig. 27. The two-dimensional scalar wave propagation in a pre-stressed membrane: the problem description and used triangular mesh.

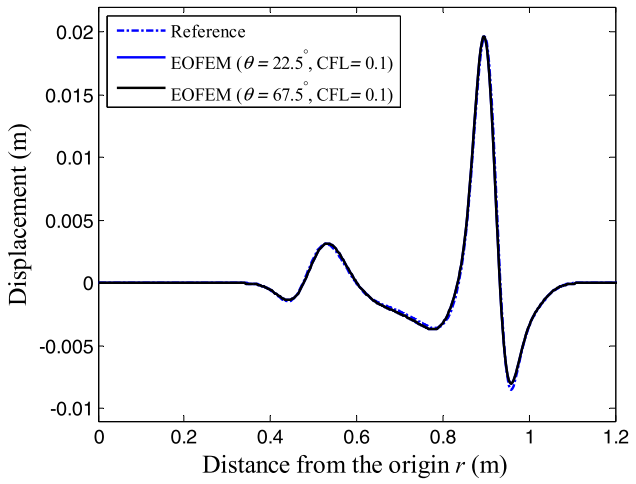

Fig. 29. Displacement distributions of the membrane along the directions $\theta = 22.5^{\circ}$ and $\theta = 67.5^{\circ}$ using the EOFEM at observation time $t = 0.8$ s.

Fig. 27: the red, black and green lines are for the directions θ=22.5°, θ=45° and θ=67.5°, respectively. In this analysis we only use the OFEM and the EOFEM. For the CFL number we use $h = 0.025$ m and $c = 1$ m/s.

The displacement solutions at observation times $t = 0.4$ s and $t = 0.7$ s using the OFEM and EOFEM with CFL = 0.1 are shown in Fig. 28 along the direction $\theta = 45^{\circ}$. The magenta lines in Fig. 28 represent the positions of the interfaces between the different media, hence we can identify the reflected and transmitted wave components in the solutions. The reference solution in the figure is obtained using the EOFEM with a very fine mesh. We see that there exist spurious oscillations in the OFEM based solutions and the EOFEM based solutions are much better.

The displacement predictions along the two other directions (θ=22.5° and θ = 67.5°) using the EOFEM at observation time $t = 0.8$ s are given in Fig. 29. We see that the present EOFEM provides almost identical results in the different wave propagation directions.

Figs. 30 and 31 give snapshots of the displacement distribution solutions obtained using the OFEM and EOFEM at different observation times and we see again that the EOFEM provides more accurate solutions.

Finally, we use decreasing CFL numbers to investigate the monotonic convergence property of the solutions. Figs. 32 and 33 give the displacement solutions along the direction $\theta = 45^{\circ}$ using the OFEM and EOFEM at observation times $t = 0.5$ s and t = 0.7 s. We find again that the EOFEM shows monotonic convergence as we decrease the CFL number.

6. Concluding remarks

We focused on employing the EOFEM with the Bathe time integration method to solve transient wave propagation problems in inhomogeneous media. We investigated the performance and properties of the approach in comparison to the use of the standard FEM and the OFEM.

A dispersion analysis shows that the total dispersion error contains contributions from the spatial discretization and the temporal discretization. As the time step size using the Bathe time integration scheme tends to zero (that is, CFL → 0), the temporal dispersion error tends to zero and the total dispersion error converges to the spatial dispersion error.

The spatial dispersion error using the standard FEM and OFEM can be large, while the EOFEM shows in the uniform mesh ana-

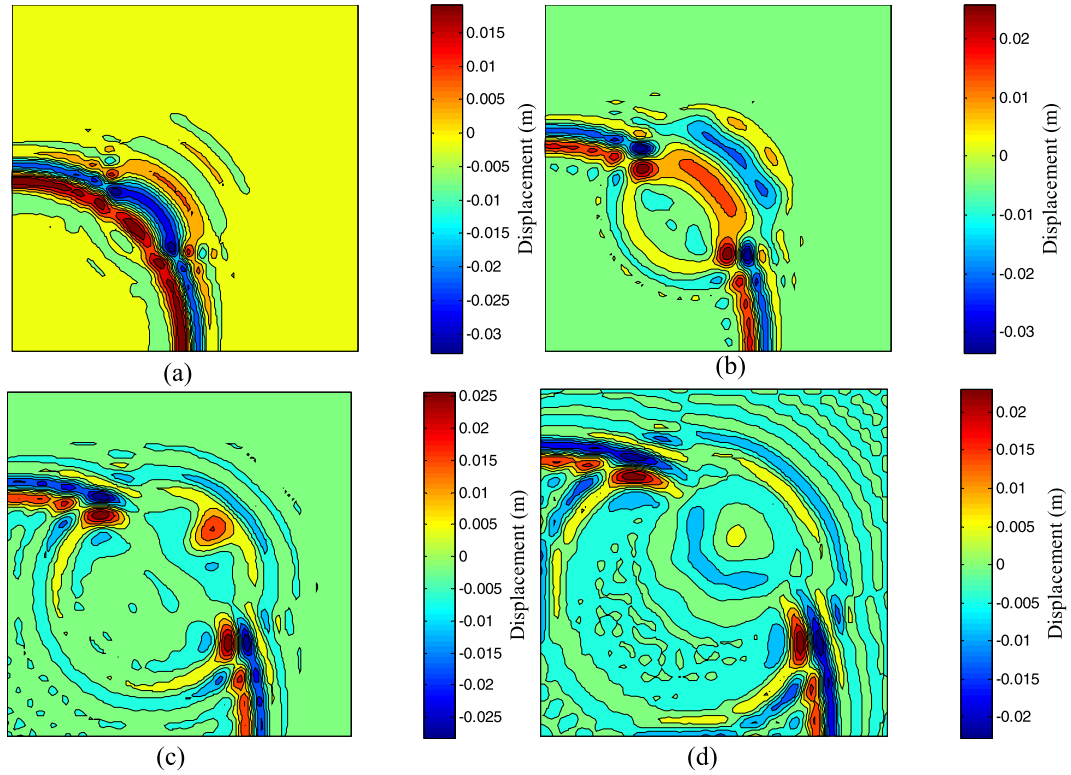

Fig. 30. Snapshots of the displacement distributions predicted using the OFEM at different observation times: (a) $t = 0.6$ s; (b) $t = 0.7$ s; (c) $t = 0.8$ s; (d) $t = 0.9$ s.

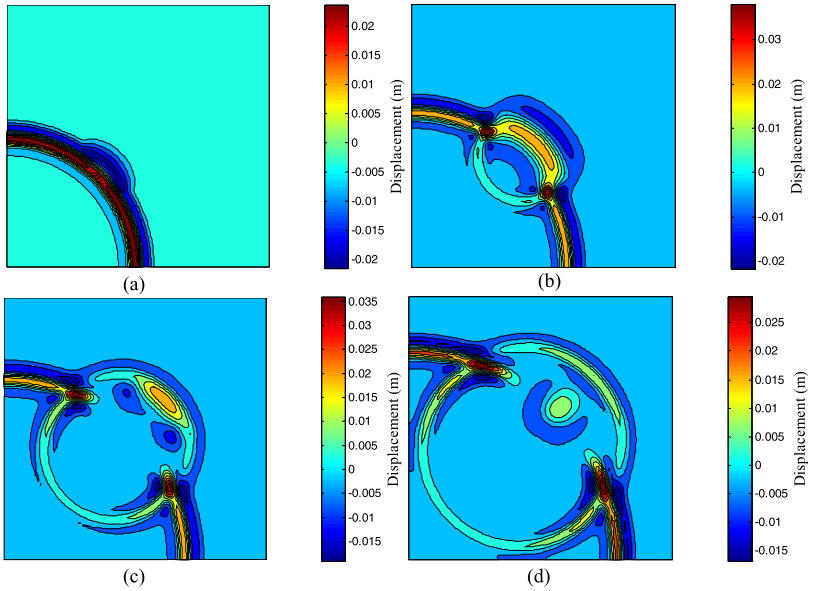

Fig. 31. Snapshots of the displacement distributions predicted using the EOFEM at different observation times: (a) $t = 0.6$ s; (b) $t = 0.7$ s; (c) $t = 0.8$ s; (d) $t = 0.9$ s.

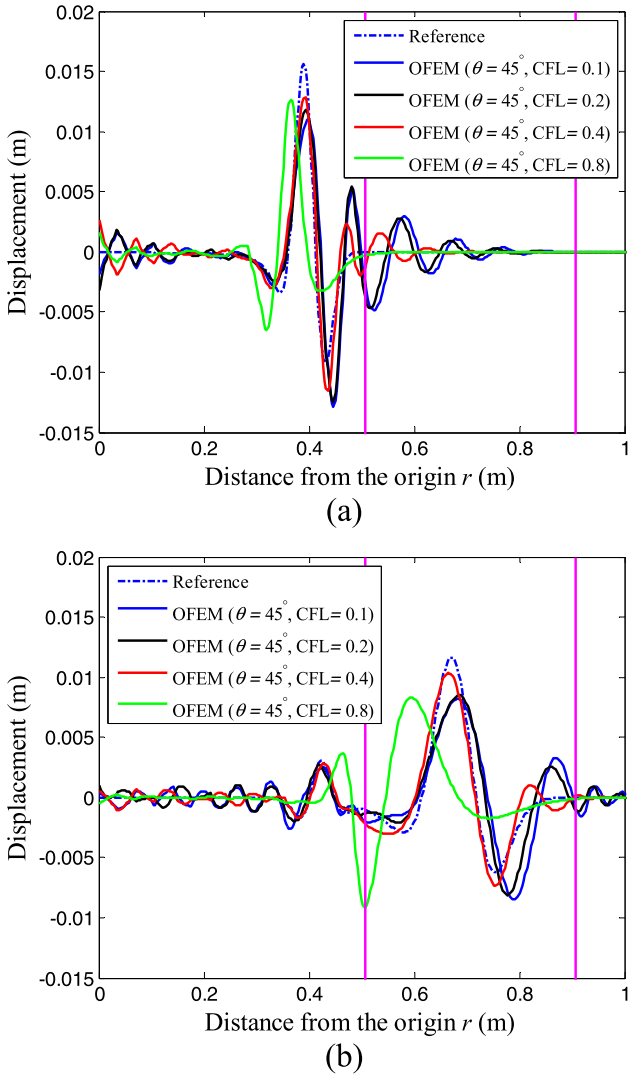

Fig. 32. Displacement distributions of the membrane along the direction $\theta = 45^{\circ}$ using the OFEM with decreasing CFL numbers: (a) observation time $t = 0.5$ s; (b) observation time $t = 0.7$ s.

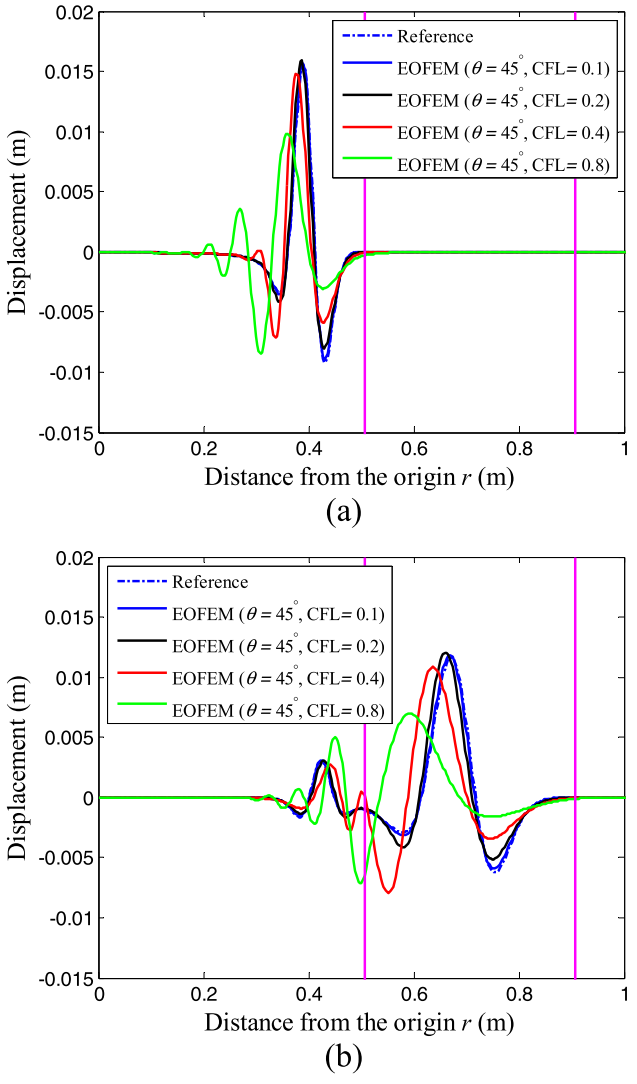

Fig. 33. Displacement distributions of the membrane along the direction $\theta = 45^{\circ}$ using the EOFEM with decreasing CFL numbers: (a) observation time $t = 0.5$ s; (b) observation time $t = 0.7$ s.

lyzed almost no spatial dispersion error for the normalized numerical wavenumber $k_h h/\pi < 1$. Hence the solution accuracy can be improved by decreasing the CFL number, and accurate results are obtained with a reasonable sufficiently fine mesh (like in static analysis using the standard finite element method). Hence the use of the EOFEM with the Bathe time integration scheme shows monotonic convergence to the exact solution for transient wave propagation problems with multiple waves, and numerical anisotropy is small, while the standard FEM and the OFEM do not display these characteristics. While we found these properties to hold for the simple problems solved, it is likely that the properties are also seen in complex analyses.

The EOFEM performs also better than the enriched FEM [14]. Due to the above good features, the EOFEM shows much promise in solving complex wave propagation problems in practical engineering, such as wave propagations in anisotropic media and multiple waves travelling in laminated composite structures.

However, there are many research tasks that are still open for investigation. We have used here only the EOEFM based on triangular element discretizations, other OFEM with enrichments might be developed and mathematical convergence analyses would be very valuable.

Declaration of Competing Interest

The authors declared that there is no conflict of interest.

Acknowledgements

We would like to thank Dr. Ki-Tae Kim, formerly in our MIT research group, for valuable comments regarding this work.

References

[1] Belytschko T, Mullen R. On dispersive properties of finite element solutions. In: Miklowitz J, Achenbach JD, editors. Modern problems in elastic wave propagation. New York (NY): Wiley; 1978. p. 67–82.
[2] Mullen R, Belytschko T. Dispersion analysis of finite element semidiscretizations of the two-dimensional wave equation. Int J Numer Meth Eng 1982;18(1):11–29.
[3] Thompson LL, Pinsky PM. A Galerkin least-squares finite element method for the two-dimensional Helmholtz equation. Int J Numer Meth Eng 1995;38(3):371–97.
[4] Deraemaeker A, Babuška I, Bouillard P. Dispersion and pollution of the FEM solution for the Helmholtz equation in one, two and three dimensions. Int J Numer Meth Eng 1999;46(4):471–99.
[5] Noh G, Ham S, Bathe KJ. Performance of an implicit time integration scheme in the analysis of wave propagations. Comput Struct 2013;123:93–105.
[6] Abboud NN, Pinsky PM. Finite element dispersion analysis for the three-dimensional second-order scalar wave equation. Int J Numer Meth Eng 1992;35(6):1183–218.
[7] Kwon S-B, Bathe KJ, Noh G. An analysis of implicit time integration schemes for wave propagations. Comput Struct 2020;230:106188. https://doi.org/10.1016/j.compstruc.2019.106188.
[8] Babuška I, Ihlenburg F, Paik ET, Sauter SA. A Generalized Finite Element Method for solving the Helmholtz equation in two dimensions with minimal pollution. Comput Methods Appl Mech Eng 1995;128(3-4):325–59.
[9] Christon MA. The influence of the mass matrix on the dispersive nature of the semi-discrete, second-order wave equation. Comput Methods Appl Mech Eng 1999;173(1-2):147–66.
[10] Guddati MN, Yue B. Modified integration rules for reducing dispersion error in finite element methods. Comput Methods Appl Mech Eng 2004;193(3-5):275–87.
[11] Ham S, Bathe KJ. A finite element method enriched for wave propagation problems. Comput Struct 2012;94-95:1–12.
[12] Ham S, Lai B, Bathe KJ. The method of finite spheres for wave propagation problems. Comput Struct 2014;142:1–14.
[13] Kim K-T, Bathe KJ. Transient implicit wave propagation dynamics with the method of finite spheres. Comput Struct 2016;173:50–60.
[14] Kim K-T, Zhang L, Bathe KJ. Transient implicit wave propagation dynamics with overlapping finite elements. Comput Struct 2018;199:18–33.
[15] Lee U, Kim J, Leung AYT. The spectral element method in structural dynamics. Shock Vib Digest 2000;32(6):451–65.
[16] Komatitsch D, Barnes C, Tromp J. Simulation of anisotropic wave propagation based upon a spectral element method. Geophysics 2000;65(4):1251–60.
[17] Chakraborty A, Gopalakrishnan S. A spectral finite element model for wave propagation analysis in laminated composite plate. J Vib Acoust 2006;128(4):477–88.
[18] Seriani G, Oliveira SP. Dispersion analysis of spectral element methods for elastic wave propagation. Wave Motion 2008;45(6):729–44.
[19] De S, Bathe KJ. The method of finite spheres. Comput Mech 2000;25(4):329–45.
[20] Lai B, Bathe KJ. The method of finite spheres in three-dimensional static analysis. Comput Struct 2016;173:161–73.
[21] Bathe KJ, Zhang L. The finite element method with overlapping elements – A new paradigm for CAD driven simulations. Comput Struct 2017;182:526–39.
[22] Zhang L, Bathe KJ. Overlapping finite elements for a new paradigm of solution. Comput Struct 2017;187:64–76.
[23] Zhang L, Kim K-T, Bathe KJ. The new paradigm of finite element solutions with overlapping elements in CAD – Computational efficiency of the procedure. Comput Struct 2018;199:1–17.
[24] Bathe KJ. The AMORE paradigm for finite element analysis. Adv Eng Softw 2019;130:1–13.
[25] Huang J, Bathe KJ. Quadrilateral overlapping elements and their use in the AMORE paradigm. Comput Struct 2019;222:25–35.
[26] Bathe KJ. Finite element procedures. 2nd ed. Watertown (MA): Prentice Hall; 2014.
[27] Bathe KJ. Conserving energy and momentum in nonlinear dynamics: A simple implicit time integration scheme. Comput Struct 2007;85(7-8):437–45.
[28] Noh G, Bathe KJ. The Bathe time integration method with controllable spectral radius: the ρ_∞-Bathe method. Comput Struct 2019;212:299–310.